Molecular Cancer

RESEARCH

Open Access

Targeting the HER2-ELF3-KRAS axis: a novel therapeutic strategy for KRAS^{G13D} colorectal cancer

Soo-Yeon Hwang[1], Yoojeong Seo[3], Seojeong Park[1], Seul-Ah Kim[1,2], Inhye Moon[1,2], Yi Liu[1], Seojeong Kim[1], Eun Seon Pak[1], Sehyun Jung[1], Hyeyoon Kim[1], Kyung-Hwa Jeon[1], Seung Hee Seo[1], Inyoung Sung[4], Heetak Lee[5], So-Yeon Park[1], Younghwa Na[6], Tae Il Kim[3] and Youngjoo Kwon[1,2*]

Abstract

Colorectal cancer (CRC) is one of the most prevalent cancers worldwide, with *KRAS* mutations playing a significant role in its tumorigenesis. Among the *KRAS* variants, the G13D mutation is associated with poor prognosis and distinctive biological behaviors. This study focuses on the role of HER2, a critical prognostic and predictive biomarker, in modulating the unique characteristics of *KRAS*^{G13D}-mutated CRCs. We identified a novel transcriptional regulatory network involving HER2, ELF3, and KRAS, with ELF3 acting as a key transcription factor (TF) that regulates KRAS expression under conditions of HER2 overexpression. Our findings reveal that this HER2-ELF3-KRAS axis is exclusively activated in *KRAS*^{G13D}, driving aggressive oncogenic features and conferring resistance to cetuximab (CTX) therapy. Through comprehensive analysis of gene expression profiles, we demonstrated that HER2 is a crucial therapeutic target specifically for *KRAS*^{G13D} CRCs. To explore this further, we introduced YK1, a small molecule inhibitor designed to disrupt the ELF3-MED23 interaction, leading to the transcriptional downregulation of HER2 and KRAS. This intervention significantly attenuated the HER2-ELF3-KRAS axis, sensitizing *KRAS*^{G13D} CRCs to CTX and reducing their tumorigenic potential by inhibiting the epithelial-to-mesenchymal transition process. Our study underscores the importance of HER2 as a key determinant in the unique biological characteristics of *KRAS*^{G13D} CRCs and highlights the therapeutic potential of targeting the HER2-ELF3-KRAS axis. By presenting YK1 as a novel pharmacological approach, we provide a promising strategy for developing tailored interventions for *KRAS*^{G13D} CRCs, contributing to the ongoing efforts in precision medicine for CRCs.

Keywords Colorectal cancer, *KRAS* mutation, *KRAS*^{G13D}, HER2, ELF3, HER2-ELF3-KRAS axis, Transcriptional regulation, Protein–protein interaction inhibitor

*Correspondence:
Youngjoo Kwon
ykwon@ewha.ac.kr
Full list of author information is available at the end of the article

Graphical Abstract

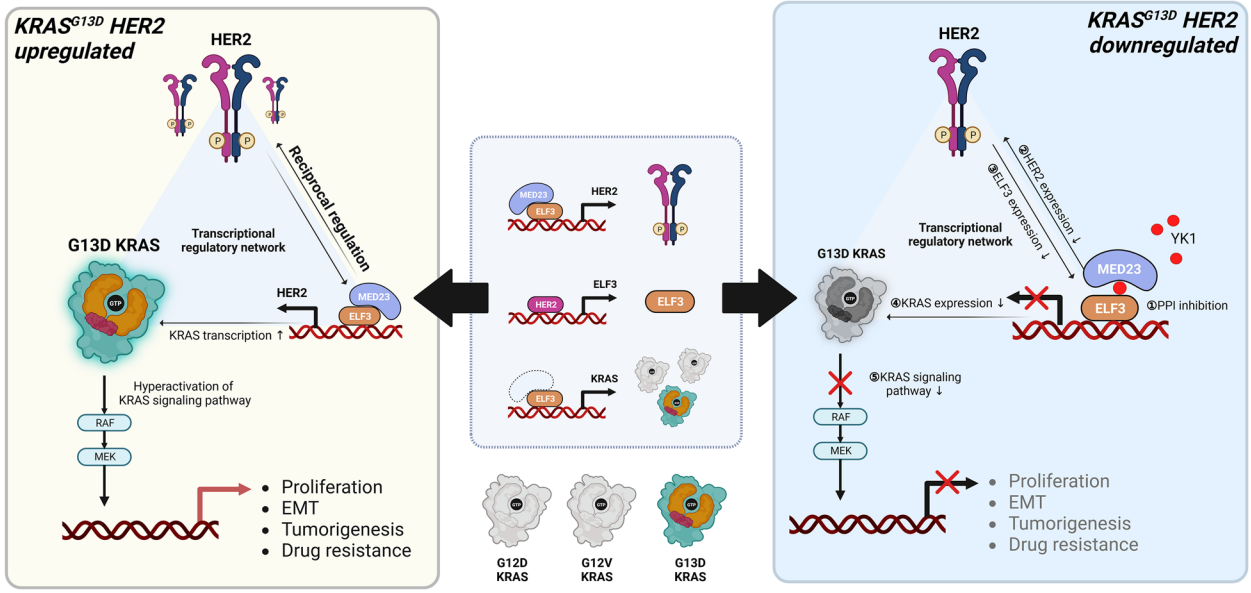

Background

Colorectal cancer (CRC), also known as large bowel or colon cancer, ranks among the most prevalent cancers globally, with an annual incidence of 1.9 million cases [1, 2]. Extensive research aimed at identifying prognostic biomarkers for CRC has greatly enhanced our understanding of the molecular alterations underlying this malignancy [3]. Among the various genetic alterations implicated in CRC tumorigenesis, mutations in the *V-Ki-ras2 Kirsten rat sarcoma viral oncogene homolog* (*KRAS*) are notably frequent in the early stage of carcinogenesis [4]. *KRAS* mutations contribute to tumor aggressiveness and are strongly associated with a poor prognosis in CRC [5]. Approximately 30–40% of CRC patients exhibit *KRAS* mutations, with 90% of these mutations concentrated in codons 12 and 13. KRAS is a crucial downstream effector of the epidermal growth factor receptor (EGFR), and mutations at these codons result in the constitutive activation of the Ras/Raf/MEK/ERK and PI3K/Akt pathways, making EGFR signaling uncontrollable [6].

Although various *KRAS* mutant variants have been reported, previous studies have not consistently considered each subtype as independent prognostic variables or predictors of therapeutic response. However, recent reports indicate that the different *KRAS* mutants exhibit distinct biological characteristics and have varying impacts on patients [7]. Notably, CRC tumors harboring the glycine-to-aspartate mutation in codon 13 (G13D) of *KRAS* display unique phenotypic characteristics. Unlike *KRAS* mutations at codon 12, the G13D variant exhibits partial sensitivity to NF1-mediated GTP hydrolysis [8, 9], suggesting that it retains some capacity to be regulated in a manner similar to $KRAS^{WT}$, though with reduced efficiency. In light of this, a subset of patients with the G13D mutation significantly benefits from anti-EGFR antibodies, such as cetuximab (CTX) [10, 11]. Despite these therapeutic advantages, multiple studies have shown that patients with the *KRAS* codon 13 mutation, particularly the G13D mutation, experience a worse prognosis compared to those with codon 12 mutations. Patients harboring the $KRAS^{G13D}$ mutation exhibit a high rate of lymph node metastasis and relatively low levels of tumor-infiltrating lymphocyte, contributing to a distinctively high recurrence rate [12, 13]. The mechanisms underlying this phenomenon remain unknown and represent a critical area for further investigation.

Human epidermal growth factor receptor 2 (HER2) is a transmembrane glycoprotein receptor with tyrosine kinase activity and is unique among the EGFR family for its ability to activate without ligand binding [14]. Through homodimerization or heterodimerization with other EGFR receptors, such as HER1, HER3, and HER4, HER2 induces phosphorylation of their tyrosine kinase domains, triggering the activation of numerous downstream signaling pathways, including RAS/RAF/ERK and PI3K/AKT/mTOR, which are closely associated with cell proliferation, differentiation, and migration [15–17]. HER2 overexpression, typically resulting from

gene amplification, leads to the constitutive activation of the downstream mitogenic signals. This uncontrolled activation contributes to aberrant cell proliferation and tumorigenesis [14, 18]. The unique activation mechanism of HER2 underscores its pivotal role in cellular signaling pathways and positions it as a significant therapeutic target in various malignancies, especially in HER2 overexpressing cancers.

Reported rates of HER2 overexpression and/or amplification vary significantly across studies, ranging from 1.6% to 47.4%, with an average frequency of approximately 5–6% [14, 17]. Although HER2 is well-established as a significant therapeutic target in breast and gastric cancers [17, 19], its overexpression and amplification are also considered as crucial prognostic and predictive markers in CRC [14, 17, 19–21], despite its relatively low incidence rate. The significance of HER2 in CRC arises from its ability to promote cell proliferation and transformation through the activation of downstream signaling pathways, as well as its role in inducing resistance to anti-EGFR agents, ultimately resulting in a poorer prognosis for patients [17, 21–25]. Recognizing the clinical importance of HER2 in CRC, trastuzumab and fam-trastuzumab deruxtecan-nxki (T-DXd) have been recently approved specifically for *KRAS/NRAS* wild-type, *BRAF* wild-type, and HER2-amplified metastatic CRCs [26].

This study demonstrates, for the first time, the clinical significance of HER2 in $KRAS^{G13D}$ mutant CRCs and elucidates how HER2 contributes to the biological uniqueness of this specific mutant subtype. We also evaluated the therapeutic relevance of regulating HER2 expression as a critical strategy to address the clinicopathological challenges associated with $KRAS^{G13D}$ CRCs. Our findings not only provide crucial insights into the interplay between HER2 and $KRAS^{G13D}$ but also propose a novel therapeutic approach, potentially steering new directions in the treatment landscape for *KRAS* mutant CRCs. This research offers a foundation for advancing precision medicine strategies tailored to the unique molecular characteristics of $KRAS^{G13D}$ CRCs, paving the way for enhanced therapeutic interventions and improved patient outcomes.

Methods

Patient specimens

We obtained total 247 CRC stage III samples by surgical resection from patients in the Severance Hospital of the Yonsei University (Seoul, Korea) between January 2011 to December 2012. Out of these, 50 patients were tested for their *KRAS* mutation status. Based on the availability of HER2 IHC staining, 41 patients were finally selected for further assessment. This sample population comprised 19 patients with *KRAS* mutations (G12C, G12D, G12S, G12V and G13D) and 22 patients with *KRAS* wild-type. None of the samples exhibited BRAF mutations. Detailed information on the patients involved in the study is summarized in Supplementary Table 1. This study received approval from Yonsei Severance Hospital.

Expression profile datasets

Publicly available gene expression datasets used for survival analysis and GSEA, including GSE39582 and GSE87211 were obtained from the National Center for Biotechnology Information (NCBI) Gene Expression Omnibus (GEO) database.

Survival analysis

In the GEO dataset analysis, samples were primarily sorted by *HER2* gene expression in descending order, irrespective of their mutation subtype. The top 33% and bottom 33% of the samples were defined as $HER2^{high}$ and $HER2^{low}$, respectively. Samples were then grouped according to *KRAS* subtype and analyzed based on mutational status or *HER2* level. Kaplan–Meier survival plots were generated for all survival analyses, with statistical significance assessed using the log-rank test. Hazard ratios (HRs) and 95% confidence intervals were measured through univariate or multivariate Cox proportional hazards regression to determine the impact of *KRAS* mutation or *HER2* level on the survival probability of each CRC patient.

Gene set enrichment assay (GSEA)

GSEA was conducted using the GSEA program provided by the Broad Institute (http://www.broadinstitute.org/gsea/index.jsp). All samples from the GSE39582 and GSE87211 datasets were first grouped according to *KRAS* mutation isotypes and then further subdivided based on *HER2* or *ELF3* expression levels (top 33%/bottom 33%) to define the phenotypes within the datasets. The 50-hallmark gene set collection from the Molecular Signatures Database (MSigDB) was used to identify gene sets highly enriched in $HER2^{high}$ patients. The number of permutations was set to 1,000. Gene sets with an FDR (False Discovery Rate) $q < 0.05$ and NOM p (Nominal *P* value) < 0.05 were considered significant. Genes that showed enrichment in the core set indicate upregulation in $HER2^{high}$ samples. The list of enriched genes for each analysis is provided in Supplementary Table 2.

Cell culture and plasmid transfection

HEK293T, a human kidney embryonic cell line (ATCC CRL-3216), and the colon cancer cell lines Caco-2 (ATCC HTB-37), HCT15 (ATCC CCL-225), HCT8 (HRT18; ATCC CCL-244), LoVo (CCL-229), and HCT116 (ATCC CCL-247) were purchased from the Korean Cell Line

Bank (KCLB, Seoul, Korea). Isogenic cell lines of SW48 were obtained from Horizon Discovery (Cambridge, UK). HEK293T and Caco-2 cells were cultured in Dulbecco's modified Eagle's medium (DMEM, Welgene, Republic of Korea) and Minimum Essential Medium (MEM, Welgene, Republic of Korea), respectively. All other cell lines were cultured in RPMI 1640 medium (Welgene, Republic of Korea). All media were supplemented with 10% fetal bovine serum (FBS, Corning®, USA) and 1% penicillin/streptomycin (Hyclone Laboratories Inc., USA). Cells were incubated in a humidified 5% CO_2 incubator at 37 °C. Media were changed every 2 to 3 days, and cells were sub-cultured at ratios of 1:5 to 1:10. All cell lines were periodically checked for mycoplasma contamination. For transient plasmid transfection, cells were plated and cultured for 24 h to reach approximately 70% confluency. Cells were then transfected with indicated plasmids using Lipofectamine® 2000 Transfection Reagent (Invitrogen, USA). Plasmids and reagents were mixed in Opti-MEM and incubated for 20 min at room temperature. Cells were then incubated for 24 h without a medium change. Antibiotics-free medium were used throughout the transfection process.

Production of lentiviral particles for HER2/ELF3 knockdown and HER2 overexpression

Lentiviral expression constructs containing shRNA targeting human HER2 or ELF3 in the pLKO.1 vector were obtained from Merck (Germany). For HER2 overexpression, the pCDH lentiviral expression vector was utilized (provided by Dr. HoGeun Yoon, Republic of Korea). For shRNA constructs, 293FT cells were transiently transfected with second-generation lentiviral packaging plasmids (VSV-G (pMDG), pRSV-REV, or pMDLg/pRRE) along with the lentiviral expression plasmid (shHER2 and/or shELF3). For HER2 overexpression, a third-generation lentivirus system was employed (PAX2, MD2, and pCDH-HER2). The supernatant containing lentiviral particles was collected 72 h post-transfection. Sequences of all the shRNAs used in this study are listed in Supplementary Table 3.

Stable cell line generation

To generate stable cell lines, cells were seeded in 6-well plates and incubated until reaching 50–60% confluency. For HER2 and ELF3 knockdown cell lines, the previously prepared lentiviral supernatant was added to the cells with polybrene at a final concentration of 8 μg/mL, and the cells were incubated for an additional 48 h. For HER2-overexpressing cell lines, cells were transfected for 24 h and then selected by adding 10 μg/mL of puromycin.

Western blot analysis

Cells were lysed in RIPA buffer (50 mM Tris, 0.25% sodium deoxycholate, 0.1% SDS, 150 mM NaCl, 1% NP-40, 1 mM EDTA and 1% protease inhibitor cocktail) (Gendepot, USA). Total protein concentration was measured using the Pierce™ BCA protein assay kit (Thermo Fisher Scientific, USA). Equal amounts of proteins (20 μg) were subjected to SDS-PAGE and transferred to a 0.2 μm PVDF membrane (Pall Life Science, USA). Membranes were blocked with 5% skim milk or 5% BSA and incubated with primary antibodies overnight at 4 °C. After washing with tris-buffered saline (TBS)−0.1% Tween20, membranes were incubated with HRP-conjugated secondary antibodies. Bands were visualized using ECL solution reagent (GE Healthcare, USA) and LAS-3000 (Fuji Photo Film Co., Ltd., Japan). Images were analyzed with Multi-Gauge Software (Fuji Photo Film Co. Ltd.). Antibodies used in this study are listed in Supplementary Table 4.

Quantitative real-time PCR

Total RNA was prepared using Tri-RNA reagent (FAVORGEN Biotech Corp., Taiwan) and complementary DNA (cDNA) was synthesized using the PrimeScript™ RT Reagent Kit (Takara Bio Inc., Japan) according to the manufacturer's instructions. Synthesized cDNAs were stored at −20 °C until further analysis. Quantitative analysis of indicated genes was performed using the SensiFAST™ SYBR No-ROX kit (Bioline, Korea) in a final reaction volume of 10 μL. PCR amplification was conducted using the CFX96 Real-time PCR detection system (Bio-Rad, Korea) with the following protocol: polymerase activation at 95 °C for 2 min, followed by 30 cycles of 95 °C for 10 s, 56 °C for 10 s, and 72 °C for 20 s. The relative quantity of mRNA was determined using the ΔΔCt method and normalized by *GAPDH* and/or *ACTIN*. Primer sequences used in this study are summarized in Supplementary Table 3.

Wound healing assay

Cells were seeded in 12-well plates and cultured until reaching over 90% confluency. A wound was created by scratching the cell monolayer with a cell scraper (SPL, Korea) and the culture medium was subsequently replaced. The cells were then incubated for an additional 24 h. Images of the wound area were captured using an Apotome laser scanning microscope (Carl Zeiss, Germany) and analyzed with Zen Pro software.

Cell viability assay

Cells were seeded in 96-well plates at a density of 1.0 $\times 10^4$ cells per well in 100 μL of growth medium. The

following day, cells were starved in FBS-free medium for 4 h and then treated with medium containing various concentrations of the test compounds for 48 h at 37 °C. Next, 10 μL of EZ-CytoX (DoGen, Korea) was added to each well. After an additional incubation for 2 h at 37 °C, absorbance was measured at 450 nm using an ELISA Microplate Reader (VersaMax, Molecular Devices, USA). IC_{50} values were determined using a four-parameter logistic equation in the Table Curve 2D program (SPSS Inc., USA).

Clonogenic assay

Cells were seeded in 6-well culture plates at a density of 2,000 cells per well. Compounds were applied immediately after seeding. Following a 10-day incubation, cells were fixed with 100% methanol for 1 h and then stained with 200 μL of crystal violet solution (1% (w/v) in absolute methanol) per well. Cells were rinsed with tap water and analyzed. Images were taken using ChemiDoc (bioimage analyzer, BR179-8280) and quantified with ImageJ software. All steps after fixation were performed at room temperature.

Luciferase assay

The predicted KRAS promoter region (−250 bp relative to the transcription starting site) was inserted into the firefly luciferase reporter pGL3-basic vector (Promega, USA). HEK293 cells were plated in 60 mm dishes and transfected with 1.0 μg of pGL3-KRAS alone or in combination with pcDNA3.1-ELF3 (provided by Dr. Seung Bae Rho, Research Institute, National Cancer Center, Republic of Korea) and 0.3 μg of β-galactosidase expression plasmid (provided by Dr. Eun-Sook Hwang, Ewha Womans University, Republic of Korea) using Lipofectamine® 2000 Transfection Reagent (Invitrogen, USA). The pGL3-basic vector was used as a negative control. After 24 h, firefly luciferase and β-galactosidase activities were measured using the Infinite M200 PRO Microplate reader (Tecan Group Ltd., Switzerland) according to the manufacturers' protocols, utilizing the Luciferase Assay System (Promega) and Galacto-Light Plus β-Galactosidase Reporter Gene Assay System (Invitrogen), respectively.

GST pull-down assay

Indicated plasmids were transduced into $SW48^{G13D}$ cells using JetPRIME® (Polyplus transfection, France). Cell lysates were prepared as described for western blot analyses [27]. Subsequently, 1000 μg of cell lysates were incubated overnight with Glutathione Sepharose™ beads (GE Healthcare, UK) at 4 °C on a rotator. The beads were then washed 3 times with ice-cold 1× PBS and eluted with a buffer containing 20 mM glutathione, 100 mM Tris–HCl (pH 8.0), 120 mM NaCl, and 10% glycerol. The precipitated proteins were analyzed via western blotting.

Tumor xenografts in nude mice

Single-cell suspensions (5×10^6 cells) of SW48 isogenic cells were subcutaneously injected into the left flank of 5-week-old athymic nude mice (Koatech, Korea). A restricted volume (100 μL) of cell suspension was slowly injected at various sites. When tumors reached 50 mm^3, the mice were randomly assigned into three groups. YK1 was dissolved in a DMAC/Tween80/saline mixture (5:10:85) and administered via intraperitoneal injection at a dose of 10 mg/kg every 3 days for 15 days. Tumor length (L) and width (l) were measured with a caliper, and tumor volume was calculated using the formula: $(L \times l^2)/2$. After sacrificing the mice, tumors were excised, and tumor weight was measured. All protocols were approved by the Institutional Animal Care and Use Committee (IACUC: 23–055) at Ewha Womans University.

Orthotopic xenografts in nude mice

Six-week-old male BALB/c nude mice (Orientbio INC, Korea) were anesthetized with isoflurane delivered via a nose cone. Afterward, a surgical incision was made in the midline of abdomen to expose the cecum, and a single-cell suspension (1×10^6 cells) of HCT15-luc (JCRB, Japan) prepared in HBSS: Matrigel (1:1) was slowly injected into the submucosal layer of the cecum using a 30-gauge needle. The injection site was monitored for leakage, and the incision was sutured. Postoperative care included cleaning the surgical area with betadine and monitoring until the mice fully recovered from anesthesia. One the total flux (p/s) values reached a specific threshold, the mice were randomly divided into three groups and administered the indicated drugs. CTX (1 mg/kg) and YK1 (20 mg/kg) were prepared in PBS and a DMSO/Tween80/saline mixture (5:5:90), respectively, and administered via intraperitoneal injection every 3 days for 15 days. Tumor growth was monitored twice a week using bioluminescent imaging with the IVIS Spectrum-CT (PerkinElmer, USA). Measurements were taken 5–7 min after intraperitoneal injection of D-luciferin (30 mg/mL). During imaging, mice were kept under isoflurane anesthesia (1–2%). After 18 days, the mice were sacrificed, and tumors were excised for histological and molecular analyses. All protocols for tumor xenograft studies were approved by the Institutional Animal Care and Use Committee (IACUC: KMEDI-23050402–00) at Preclinical Research Center of Daegu-Gyeongbuk Medical Innovation Foundation.

Immunohistochemistry (IHC) assay for patient samples and xenograft mouse model

We obtained total 165 CRC stage III samples by surgical resection from Severance Hospital of the Yonsei University (Seoul, Korea) between January 2011 to December 2012 (IRB#4–2012-0859). Among them, 41 of metastatic recurrent CRC patient tissue specimens were prepared in 4 μm-thick sections from formalin-fixed, paraffin-embedded tissue blocks. Sections were deparaffinized in xylene and rehydrated in a series of gradually decreasing ethanol concentrations. Antigen retrieval was performed using sodium citrate buffer (10 mM, pH 6.0) in a heated pressure cooker for 5 min. Sections were then incubated with 3% hydrogen peroxide for 30 min to block endogenous peroxidase activity, followed by a blocking reagent for 30 min at room temperature. Primary antibodies (HER2, E-cadherin and vimentin) were applied and incubated overnight at 4 °C, followed by incubation with secondary antibodies for 30 min at room temperature. Slides were developed using a Vectastain ABC kit (Vector Laboratories), and immunostained with DAB solution (Dako, Carpinteria, CA). After counterstaining with hematoxylin, IHC staining was evaluated using light microscopy at 100 ×magnification. Tumors from the xenograft mouse model were fixed in 10% NBF and prepared as paraffin block sections for IHC. Antibodies were incubated using an automatic IHC staining instrument (Ventana, Tucson, AZ, USA) according to the manufacturer's protocols. IHC staining was evaluated semi-quantitatively using an IHC score, calculated by multiplying the intensity by the fraction score (percentage of samples at each scale), resulting in a range from 0 to 300. All imaging and assessments were performed using an Axiophot 2 apparatus (Carl Zeiss MicroImaging Inc., USA). The antibodies and their dilution ratios are listed in Supplementary Table 4.

Statistical analysis

Statistical analyses were performed using GraphPad Prism 10 software (GraphPad Software, Inc., La Jolla, CA, USA). For the evaluation of two datasets, unpaired Student's t-tests or Mann–Whitney tests were conducted; for comparisons involving more than two groups, one-way or two-way analysis of variance (ANOVA) was used. Each experiment was conducted at least in triplicate to ensure reliability. All calculated *p*-values were two-sided, with $p < 0.05$ considered statistically significant.

Results

HER2 as a key determinant of unique biological characteristics of *KRAS*^{G13D} CRCs

The role of *KRAS* mutations as adverse prognostic factors in CRC is well-established, with different subtypes exerting varied effects on patient survival [7, 28–31]. To validate these distinct impacts, we initially analyzed the gene expression profile of 437 tumor samples from CRC patients using the publicly available Gene Expression Omnibus (GEO) dataset (GSE39582). Patients with the *KRAS*^{G13D} mutation exhibited significantly lower survival probability compared to those with *KRAS*^{WT} (log-rank test, $p = 0.0113$; hazard ratio, HR = 1.86) or other *KRAS* mutations (HR = 1.15) (Fig. 1A).

To assess the prognostic significance of HER2 expression across different *KRAS* mutation subtypes, we stratified the patient samples based on their HER2 expression levels (HER2^{high} and HER2^{low}) and compared their survival probabilities (Fig. 1B-D). Our findings revealed heterogeneous associations between HER2 expression and patient outcomes across *KRAS* mutation subtypes. Notably, patients with *KRAS*^{G13D} and HER2^{high} had lower overall survival (OS) compared to those with *KRAS*^{G13D} and HER2^{low} (HR = 3.769; 95% CI, 0.84–16.94; $p = 0.039$) (Fig. 1B). In contrast, patients harboring *KRAS*^{G12} variants or *KRAS*^{WT} showed no statistically significant association with survival probability or even better OS with HER2^{high} (*KRAS*^{G12}; HR = 0.60; 95% CI, 0.255–1.41; $p = 0.247$, *KRAS*^{WT}; HR = 0.54; 95% CI, 0.32–0.87; $p = 0.0146$) (Fig. 1C and D). This mutation subtype-specific relationship underscores the potential of HER2 as a prognostic biomarker specifically in *KRAS*^{G13D}-mutated CRCs.

For further confirmation, we retrospectively analyzed the OS of 247 grade III CRC patients from Severance Hospital (Yonsei University) based on their *KRAS* mutation status. Out of the 247 patient tissues, 50 were tested for mutations, and finally 41 patient tissues possessing acceptable HER2 IHC staining availability were selected for analysis. These 41 patients were categorized into three groups: group 1–*KRAS*^{WT} ($n = 22$); group 2–*KRAS*^{G13D} variants [*KRAS*$^{G12/13}$ double mutants ($n = 11$) and *KRAS*^{G13D} single mutant ($n = 1$)]; and group 3–*KRAS*^{G12} variants ($n = 7$); and (Supplementary Fig. 1A). Consistent with the database analysis result, the 5-year survival rate of group 2 patients was significantly lower than that of group 3, supporting the negative prognostic significance of the *KRAS*^{G13D} mutation in CRC patients (log-rank test, $p = 0.0387$) (Supplementary Fig. 1B). We further subdivided these patients into HER2^{high} and HER2^{low} groups and found that the 5-year survival rate of HER2^{high} group 2 patients was distinctively lower than that of group 1 and 3 ($p = 0.0387$), suggesting that HER2 overproduction is a critical risk factor specifically for *KRAS*^{G13D} CRC patients (Supplementary Fig. 1C).

Although reported values vary across studies, EGFR overexpression has been observed in up to 80–90% of CRC patients [32], while mutations in the EGFR gene itself are rare [33]. Consequently, CTX has long been widely used as a first-line therapy for CRC patients.

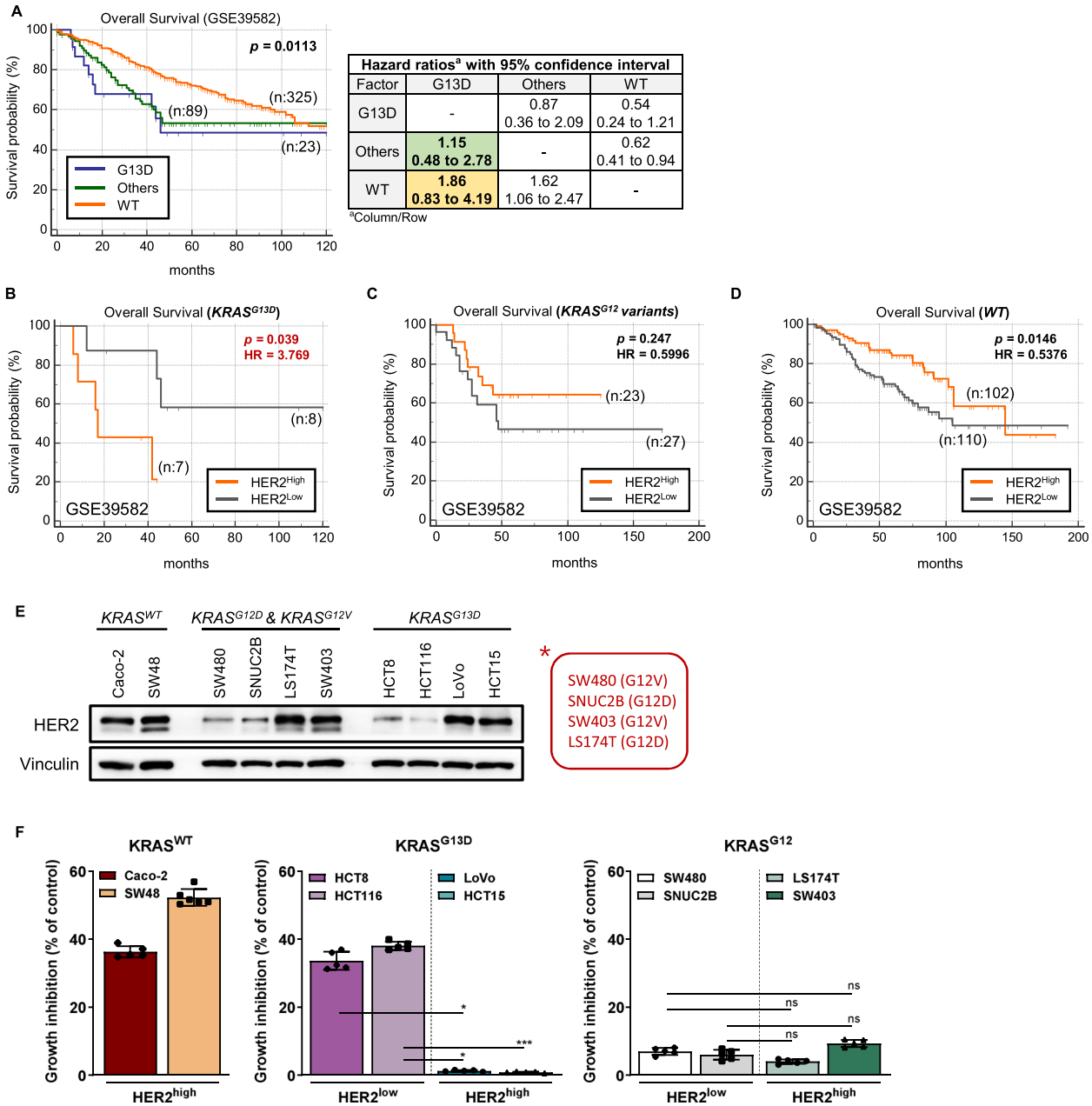

Hazard ratios[a] with 95% confidence interval			
Factor	G13D	Others	WT
G13D	-	0.87 0.36 to 2.09	0.54 0.24 to 1.21
Others	**1.15** **0.48 to 2.78**	-	0.62 0.41 to 0.94
WT	**1.86** **0.83 to 4.19**	1.62 1.06 to 2.47	-

[a]Column/Row

Fig. 1 HER2 as a potential key determinant of the unique biological characteristics of *KRAS*^{G13D} CRCs. **A** The overall survival rate of patients with different *KRAS* mutation statuses was assessed using the GSE39582 database, which included a total of 578 patients ($^{**}p < 0.01$, log-rank test). **B-D** The prognostic significance of HER2 was evaluated by comparing the overall survival probabilities between HER2^{high} and HER2^{low} subgroups in *KRAS*^{G13D} ($n = 15$) (B), *KRAS*^{G12} variant ($n = 212$) (C) and *KRAS*^{WT} ($n = 50$) (D) CRC patients (GSE39582). ($^{*}p < 0.05$, log-rank test). The hazard ratio for each independent variable was calculated by multivariate Cox proportional hazard regression. **E** The expression levels of HER2 were measured in various CRC cell lines with different *KRAS* mutation statuses. **F** The growth inhibitory effect of CTX (20 μg/mL) was tested against diverse CRC cell lines with different *KRAS* mutation statuses following 48 h-treatment at the indicated concentrations

However its use is typically limited to patients harboring *KRAS*^{WT} tumors, as RAS mutations have been shown to significantly reduce CTX effectiveness [34, 35]. Nevertheless, some studies have indicated that a subset of CRC patients with the *KRAS*^{G13D} mutation respond to CTX, exhibiting improvements in overall and progression-free survivals [36, 37]. Given that HER2 levels serve as a key prognostic factor for the *KRAS*^{G13D} CRCs, we sought to explore whether HER2 levels are also associated with CTX responsiveness in CRCs with different *KRAS*

variants. To this end, we selected several CRC cell lines harboring different *KRAS* mutations and first assessed their HER2 expression levels (Fig. 1E). Known CTX-sensitive $KRAS^{WT}$ CRC cell lines, SW48 and Caco-2, were used as controls to compare the susceptibility of each cell line to CTX. Remarkably, a distinct trend of higher HER2 levels and lower CTX sensitivity was observed exclusively in cells with $KRAS^{G13D}$ mutation (Fig. 1F). The two $KRAS^{G13D}$ $HER2^{low}$ cell lines, HCT8 and HCT116, showed significant sensitivity to CTX (20 μg/mL), comparable to the $KRAS^{WT}$ CRC cell lines, while the other two $KRAS^{G13D}$ $HER2^{high}$ cell lines, LoVo and HCT15, demonstrated relative resistance to CTX at the same concentration (Fig. 1F, Supplementary Fig. 1D and E). Consistently, CTX treatment downregulated phospho-EGFR (p-EGFR) and the downstream signaling pathway in a concentration-dependent manner in $KRAS^{G13D}$ $HER2^{low}$ cells, similar to the $KRAS^{WT}$ controls (Supplementary Fig. 1D), resulting in significant inhibition of cell growth and proliferation (Fig. 1F and Supplementary Fig. 1E). Conversely, cells with $KRAS^{G12}$ variants showed resistance to CTX regardless of their HER2 expression levels (Fig. 1F and Supplementary Fig. 1D). These findings suggest that HER2 may serve as a determinant for CTX sensitivity in $KRAS^{G13D}$ CRCs.

HER2 expression as a key predictor of CTX susceptibility in $KRAS^{G13D}$ CRC cells

To further investigate whether HER2 expression levels are crucial in determining the susceptibility of $KRAS^{G13D}$ CRC cells to CTX, we employed four SW48 ($KRAS^{WT}$, $HER2^{high}$) isogenic cell lines harboring different *KRAS* mutations ($SW48^{WT}$, $SW48^{G12D}$, $SW48^{G12V}$ and $SW48^{G13D}$) and generated their corresponding HER2 knockdown clones (WT_shHER2, G12D_shHER2, G12 V_shHER2, and G13D_shHER2). As expected, the isogenic *KRAS* mutant cell lines showed reduced CTX responsiveness compared to the parental $SW48^{WT}$ cells (Fig. 2A-H). However, HER2 silencing had varying effects on CTX responsiveness across the isogenic cell lines (Fig. 2A-I). While both G12D_shHER2 and G12V_shHER2 cells showed no significant differences in CTX-induced growth inhibition and long-term proliferation compared to their parental cells (Fig. 2C-F), the G13D_shHER2 clone intriguingly regained CTX sensitivity (Fig. 2G and H), exhibiting an even higher response rate than the $SW48^{WT}$ cells. These findings were further corroborated by tumor volume reduction observed exclusively in G13D_shHER2 xenografted mice (Fig. 2I), collectively indicating that HER2 is a critical determinant of CTX sensitivity, particularly in $KRAS^{G13D}$ CRC cells, but not in those with G12 mutations.

Further evaluation with HCT15 ($KRAS^{G13D}$, $HER2^{high}$) cells confirmed that HER2 knockdown (HCT15_shHER2) significantly sensitized the cells to CTX. In HCT15_shHER2 cells, CTX exhibited remarkable growth inhibitory (Fig. 2J) and anti-proliferative effects (Fig. 2K), comparable to those in CTX-sensitive Caco-2 ($KRAS^{WT}$, $HER2^{high}$) cells, but not in HCT15_shCTRL cells. Conversely, inducing HER2 overexpression in the HCT116 ($KRAS^{G13D}$, $HER2^{low}$) cell line enhanced resistance to CTX (Supplementary Fig. 2 A and B), further validating the critical role of HER2 overexpression in the resistance of $KRAS^{G13D}$ CRCs to CTX. Additionally, transient transduction of $KRAS^{G13D}$ into Caco-2 ($KRAS^{WT}$, $HER2^{high}$) cells led to a complete loss of sensitivity to CTX, with no detectable changes in downstream signaling molecules AKT and MAPK phosphorylation. However, stable HER2 silencing negated the $KRAS^{G13D}$-induced resistance to CTX and preserved the CTX-mediated inhibition of the signaling pathway (Fig. 2L). These results underscore the pivotal role of HER2 in modulating the CTX response in $KRAS^{G13D}$ CRC cells.

HER2 expression drives aggressive oncogenic features in $KRAS^{G13D}$ CRC cells

To confirm HER2 as a key driver of the aggressive oncogenic features in $KRAS^{G13D}$ CRCs, we compared cell

(See figure on next page.)

Fig. 2 HER2 expression level as a key predictive factor for the susceptibility of $KRAS^{G13D}$ CRC cells to CTX. **A-H** The inhibitory effects of CTX on cell growth (**A**, **C**, **E**, and **G**) and colony forming ability (**B**, **D**, **F**, and **H**) were evaluated in SW48 isogenic cell lines and their HER2-knockdown (KD) clones: WT_shCTRL/WT_shHER2 (**A**, **B**), G12D_shCTRL/G12D_shHER2 (**C**, **D**), G12 V_shCTRL/G12V_shHER2 (**E**, **F**), and G13D_shCTRL/G13D_shHER2 (**G**, **H**). 24 h treatment was conducted for growth inhibition ($n = 6$) and a 10 day treatment for long-term anti-proliferative effects ($n = 5$) at the indicated concentrations (ANOVA, ns = non-significant, $^{****}p < 0.0001$ vs. shCTRL). **I** The tumor growth inhibitory effect of CTX (intraperitoneal injection at 1 mg/kg every 3 days) was evaluated using xenograft mouse models of SW48 isogenic cell lines and their HER2-silenced clones ($n = 5$ per group) (ANOVA, $^{***}p < 0.001$ vs. CON). **J** The growth inhibitory effect of CTX was tested against HCT15 (HCT15_shCTRL) and its HER2 knockdown clone (HCT15_shHER2), with caco-2 serving as a positive control ($n = 4$). 24 h-treatment was conducted at the indicated concentrations. **K** The long-term anti-proliferative effect of CTX was assessed against HCT15_shCTRL and HCT15_shHER2 cells ($n = 5$) following 10 d-treatment at the indicated concentrations (ANOVA, ns = non-significant, $^{***}p < 0.001$, $^{****}p < 0.0001$ vs. control (0), $^{\#\#\#\#}p < 0.0001$ vs. shCTRL). **L** Changes in CTX sensitivity were assessed in Caco-2 and HER2-KD Caco-2 cells transduced with $KRAS^{G13D}$ using pcDNA4-$KRAS^{G13D}$-Hismax construct following 16 h-treatment at the indicated concentrations

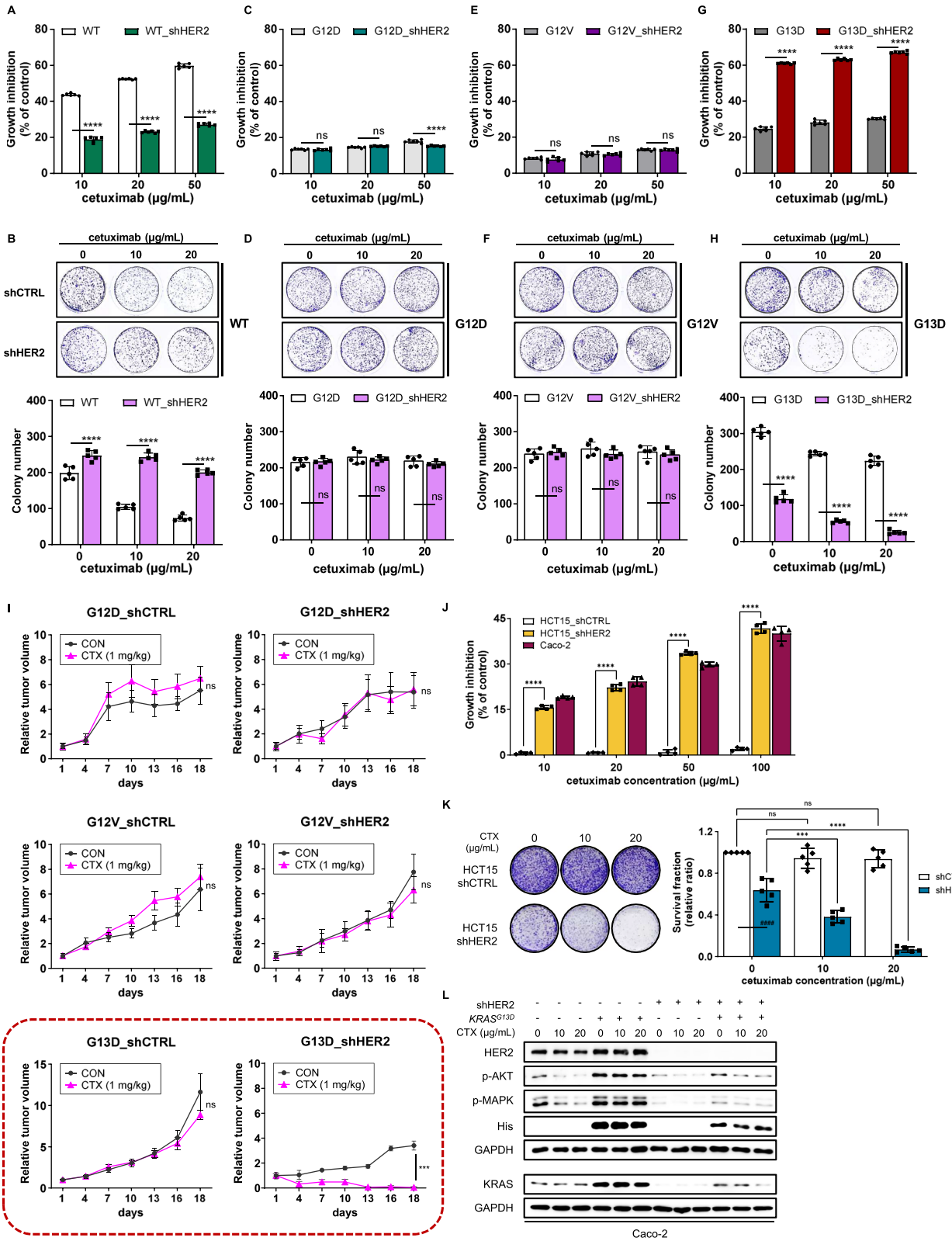

Fig. 2 (See legend on previous page.)

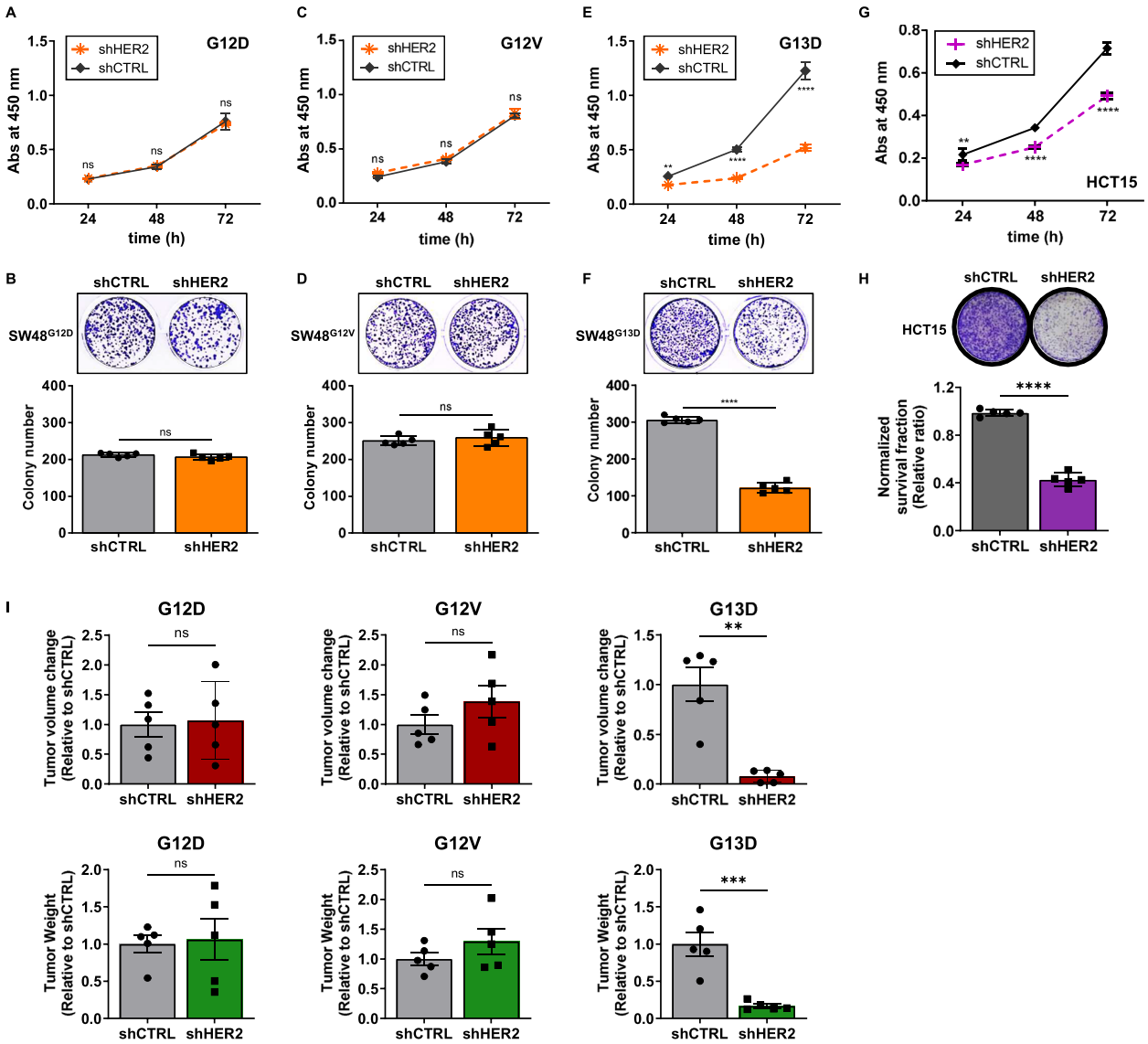

Fig. 3 Highly-expressed HER2 as a critical inducer of aggressive oncogenic features in *KRAS*^{G13D} CRC cells. **A-F** The cell growth rate (**A**, **C**, and **E**) and colony-forming ability (**B**, **D**, and **F**) of SW48 isogenic cell lines and their HER2-knockdown (KD) clones were evaluated: G12D_shCTRL/G12D_shHER2 (**A**, **B**), G12V_shCTRL/G12V_shHER2 (**C**, **D**), and G13D_shCTRL/G13D_shHER2 (**E**, **F**). The cell growth rate was assessed over short-term periods at the indicated time points ($n = 5$), while the colony formation rate was tested over 10 days ($n = 5$) (ANOVA was used for the cell growth rate analysis and Student's t-test for the colony formation rate, ns = non-significant, $^{**}p < 0.01$, $^{****}p < 0.0001$ vs. shCTRL). **G**, **H** The growth rates (**G**) and long-term cell proliferation rates (**H**) of HCT15 (HCT15_shCTRL) and its HER2-silenced model (HCT15_shHER2) were evaluated. For growth rate evaluation, each cell line was monitored up to 72 h ($n = 5$), and cell viability at each time point was colorimetrically assessed by absorbance at 450 nm. For the cell proliferation rate assessment, both cell lines were incubated for 10 days ($n = 5$) (ANOVA was used for (**G**) and Student's t-test for (**H**), ns = non-significant, $^{**}p < 0.01$, $^{****}p < 0.0001$ vs. shCTRL). **I** Tumor forming abilities of SW48 isogenic cell lines and their HER2-KD clones were evaluated using xenograft mouse models. Each cell line pair (shCTRL and shHER2) was separately injected to the left or right side of the mouse flank and tumor growth was monitored for a total of 30 days ($n = 5$). Both changes in tumor volume and tumor weight data were presented as relative ratios to shCTRL (Student's t-test, ns = non-significant, $^{**}p < 0.01$, $^{***}p < 0.001$ vs. shCTRL)

growth and long-term proliferation rates among isogenic cell lines and their corresponding HER2 knockdown clones (Fig. 3A-H). Our findings revealed that HER2 depletion had varying effects on *KRAS*^{G12} variant and *KRAS*^{G13D} cell lines. Specifically, stable HER2 silencing in SW48^{G12D} and SW48^{G12V} cells resulted in no significant changes (Fig. 3A-D), whereas the same silencing in SW48^{G13D} cells led to a marked reduction in cellular growth and long-term proliferation (Fig. 3E and F). These results were further validated in

HCT15_shHER2 and HER2 overexpression-induced HCT116 ($KRAS^{G13D}$, $HER2^{low}$) cells, where HER2 knockdown or overexpression notably decreased or increased both growth and proliferation rates in $KRAS^{G13D}$-harboring CRC cells, respectively (Fig. 3G, H, Supplementary Fig. 3A, B). Consistently, HER2 depletion did not reduce the tumorigenic potential of $SW48^{G12D}$ and $SW48^{G12V}$ cells when implanted into the flanks of athymic nude mice, but it nearly completely abrogated the tumor-forming capacity of $SW48^{G13D}$ cells (Fig. 3I). This highlights HER2 as a relevant therapeutic target, specifically in $KRAS^{G13D}$ CRC subtypes.

EMT process is distinctively engaged in $KRAS^{G13D}$CRCs with high HER2 levels

To understand how highly expressed HER2 specifically enhances the aggressiveness of $KRAS^{G13D}$ CRCs contributing to poor prognosis, we conducted a Gene Set Enrichment Assay (GSEA) using the Molecular Signatures Database (MSigDB) Hallmark gene set collection. Analyzing data from GSE39582, we found that $KRAS^{G13D}$

A $KRAS^{G13D}$

RANK	NAME	SIZE	NES	NOM p-val	FDR q-val
1	EPITHELIAL_MESENCHYMAL_TRANSITION	192	6.13	0	0
2	APICAL_JUNCTION	193	3.86	0	0
3	MYOGENESIS	196	3.52	0	0
4	MITOTIC_SPINDLE	185	3.16	0	0
5	UV_RESPONSE_DN	135	2.93	0	0
6	INTERFERON_GAMMA_RESPONSE	187	2.91	0	0
7	HYPOXIA	188	2.78	0	1.43E-04
8	INTERFERON_ALPHA_RESPONSE	88	2.56	0	4.06E-04
9	COAGULATION	133	2.44	0.0030	0.0013
10	ESTROGEN_RESPONSE_EARLY	183	2.39	0	0.0016
11	P53_PATHWAY	182	2.37	0	0.002
12	MTORC1_SIGNALING	183	2.22	0	0.004
13	G2M_CHECKPOINT	178	2.01	0.004	0.014
14	KRAS_SIGNALING_UP	192	1.91	0.017	0.023
15	ESTROGEN_RESPONSE_LATE	194	1.90	0.006	0.024
16	COMPLEMENT	192	1.89	0.013	0.024
17	HEDGEHOG_SIGNALING	35	1.79	0.010	0.039
18	CHOLESTEROL_HOMEOSTASIS	71	1.79	0.019	0.037

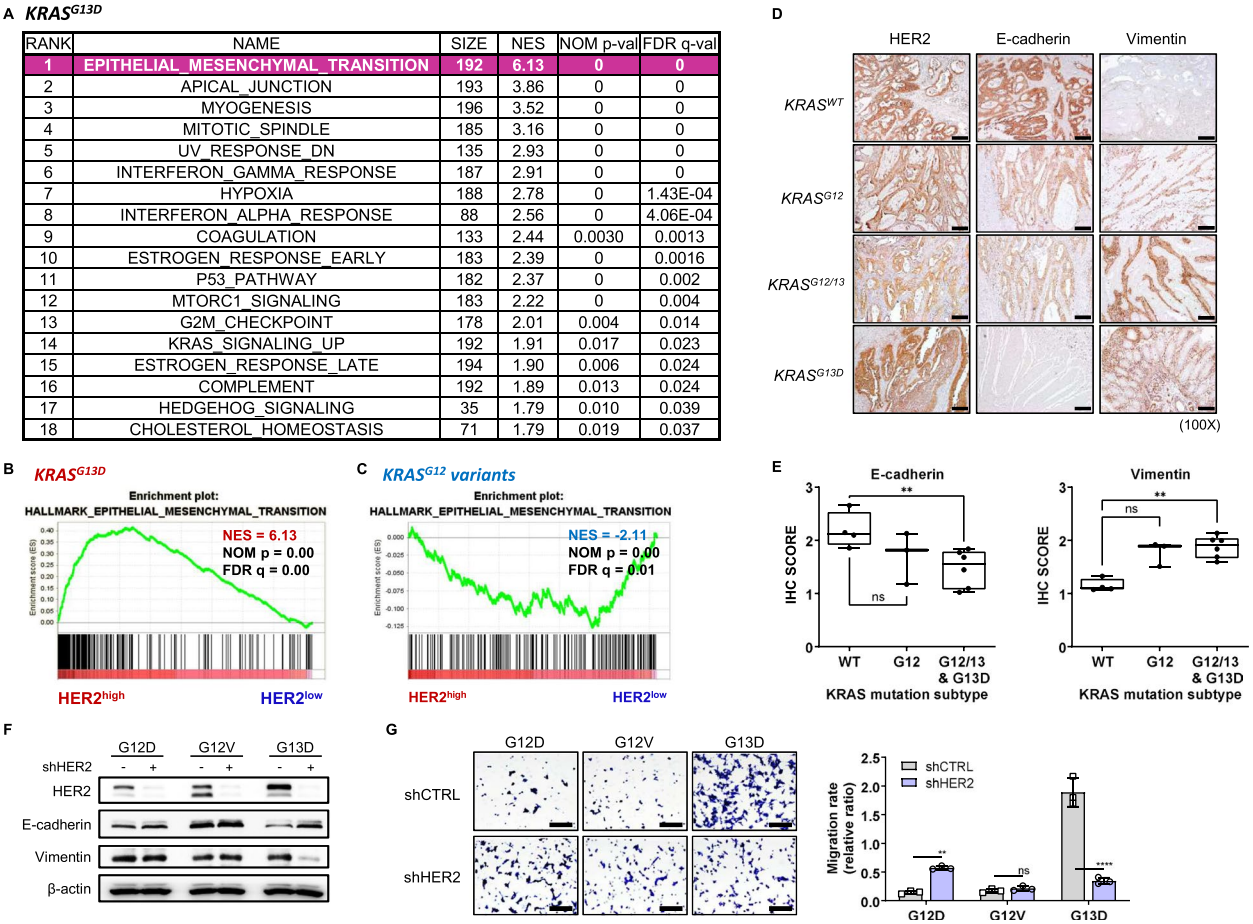

Fig. 4 EMT as a process distinctively engaged in $KRAS^{G13D}$ CRCs with high HER2 levels. **A** GSEA was conducted on the expression dataset of $KRAS^{G13D}$ CRC patient samples from GSE39582 using a pre-annotated hallmark gene set collection, with FDR $q < 0.05$ and NOM $p < 0.05$ considered significant. **B**, **C** GSEA plots for the EMT gene set were generated using the expression datasets of $KRAS^{G13D}$ CRC (**B**) and $KRAS^{G12}$ CRC (**C**) patient samples from GSE39582. The datasets were reconstituted based on HER2 expression levels. NES, NOM p and FDR q values are as displayed above. **D** Representative IHC images of HER2, E-cadherin, and vimentin for HER2 high tumors with different KRAS mutational statuses are shown (I, $KRAS^{WT}$; II, $KRAS^{G12}$; III, $KRAS^{G12/13}$; and IV, $KRAS^{G13D}$). Images are at 100 × magnification (scale bars = 200 μm). **E** IHC scores of E-cadherin and vimentin were calculated by intensity score × fraction score, with quantification performed using ImageJ software. Box-and-Whisker plots were used to compare the distribution of each sample within the groups (ANOVA, ns = non-significant, $^{**}p < 0.01$). **F** HER2-mediated changes in the expression levels of E-cadherin and vimentin were evaluated in various SW48 isogenic cell lines. **G** Transwell migration assay was performed on shCTRL and shHER2 clones of SW48 isogenic cell lines, with images at 200 × magnification (scale bars = 100 μm). Quantification was conducted through ImageJ software, presenting the rates as relative ratios to shCTRL for each cell line ($n = 3$) (ANOVA, ns = non-significant, $^{**}p < 0.01$, $^{****}p < 0.0001$ vs. shCTRL)

HER2^{high} CRCs were significantly enriched in the epithelial-to-mesenchymal transition (EMT) gene signature (Fig. 4A, B, Supplementary Table 2), a process that increases cell motility by acquiring mesenchymal traits and losing epithelial properties. In contrast, *KRAS*^{G12} HER2^{high} CRCs did not exhibit this enrichment (Supplementary Fig. 4A). Similar findings were confirmed in *KRAS*^{G13D} HER2^{high} patients from the GSE87211 database (Supplementary Fig. 4B). The *KRAS*^{G12} HER2^{high} group, in fact, showed a negative correlation with EMT (Fig. 4C) and different enrichment patterns compared to the *KRAS*^{G13D}-harboring subgroup (Supplementary Fig. 4A), suggesting that codon-specific signaling drives unique biological effects.

Comparative analysis revealed that HER2^{high} CRC patient samples with *KRAS*^{G13D} exhibited significantly lower level of the epithelial marker E-cadherin and higher level of the mesenchymal marker vimentin compared to other KRAS isoforms (Fig. 4D, E, Supplementary Fig. 4C, D). Even within the *KRAS*^{G13D}-harboring subgroup, the HER2^{high} patients had lower E-cadherin and higher vimentin levels compared to HER2^{low} patients, further demonstrating the oncogenic role of HER2 in *KRAS*^{G13D} CRCs (Supplementary Fig. 4C, D). Moreover, HER2 knockdown specifically attenuated the EMT process in SW48^{G13D}, upregulating E-cadherin and downregulating vimentin, while no such alterations were observed in shHER2 clones of SW48^{G12D} and SW48^{G12V} cells (Fig. 4F), indicating that HER2 is crucial in *KRAS*^{G13D} CRCs but not in *KRAS*^{G12} CRCs. In line with this, cell migration potential was significantly higher in SW48^{G13D} cells compared to other isogenic subtypes, and this was notably reduced by HER2 silencing (Fig. 4G).

To further verify the association between HER2 and EMT in CRCs carrying the *KRAS*^{G13D} mutation, we examined the protein and mRNA expression levels of mesenchymal markers (N-cadherin and vimentin) and epithelial markers (E-cadherin, occludin, and CK18) in four *KRAS*^{G13D} mutant cell lines (HCT8, HCT116, LoVo, and HCT15). HER2^{high} cells (LoVo, HCT15) exhibited higher mesenchymal marker levels and lower epithelial markers levels compared to HER2^{low} cells (HCT8 and HCT116) (Supplementary Fig. 4E, F). Moreover, HER2 overexpression in HER2^{low} cell lines markedly increased mesenchymal markers and decreased epithelial markers (Supplementary Fig. 4G), while HER2 knockdown in HER2^{high} cell lines produced the opposite effects (Supplementary Fig. 4H). Consistently, EMT marker expression was significantly elevated in response to *KRAS*^{G13D} transduction in *KRAS*^{WT} Caco-2 cells. However, stable HER2 silencing in Caco-2 cells prevented transduction of *KRAS*^{G13D} from altering EMT marker expression (Supplementary Fig. 4I). These observations demonstrate that HER2 is an oncogenic factor that specifically drives EMT in the presence of the *KRAS*^{G13D} mutation. Consequently, shHER2-mediated shift from the mesenchymal to epithelial state in HCT15 cells resulted in morphological changes from a spindle-like to a more cobblestone-like shape, with a significant increase in cell circularity (Supplementary Fig. 4J). HER2 blockade also remarkably decreased the cell motility (Supplementary Fig. 4K), overall authenticating the vital role of HER2 as an inducer of aggressive oncogenic features in *KRAS*^{G13D} CRCs.

Transcriptional regulatory axis of HER2-ELF3-KRAS as a therapeutic target for *KRAS*^{G13D}CRCs

Building on our findings that HER2 is a predictive biomarker and prognostic factor for CTX response in *KRAS*^{G13D} CRCs, we investigated potential strategies to regulate HER2 as a novel therapeutic approach for CRC patients harboring the *KRAS*^{G13D} mutation. Trastuzumab, an FDA-approved HER2-targeting monoclonal antibody drug, was first tested on three *KRAS*^{G13D}, HER2^{high} CRC cell lines (SW48^{G13D}, HCT15 and LoVo). Despite high HER2 expression, trastuzumab showed no impact on colony formation or HER signaling pathways (Fig. 5A, B). This suggests that targeting the already overexpressed HER2 protein on the cell membrane is insufficient to elicit anticancer effects in *KRAS*^{G13D}, HER2^{high} CRCs. Meanwhile, shRNA-mediated stable HER2 silencing significantly downregulated direct downstream molecules, such as p-AKT (Fig. 5C), leading to substantial anti-proliferative effects against *KRAS*^{G13D} CRCs (Fig. 3G-J).

Notably, HER2 knockdown led to a significant decrease in KRAS protein levels across all three cell lines (SW48^{G13D}_shHER2, HCT15_shHER2, and LoVo_shHER2) (Fig. 5C), unlike trastuzumab treatment (Fig. 5B, Supplementary Fig. 5A). This reduction was confirmed to be due to mRNA downregulation (Fig. 5D) rather than protein degradation (Supplementary Fig. 5B). These findings prompted us to hypothesize that a specific transcription factor (TF), regulated by HER2, may directly influence KRAS expression, particularly considering that HER2 can localize to the nucleus and demonstrate transcriptional activity [38]. To explore this, we first used the Biological General Repository for Interaction Datasets (BioGRID) database [39], identifying 471 molecules that either physically or genetically interact with HER2 (Fig. 5E). Simultaneously, through further analysis using the Gene Transcription Regulation Database (GTRD) [40, 41], we uncovered 218 potential TFs capable of binding to the KRAS promoter region (−250 bp relative to transcription starting site) (Fig. 5E, Supplementary Fig. 5C). Among them, seven TFs– ELF3, ESR1, MYC, SMAD1, STAT1, STAT3, and TP53–emerged as

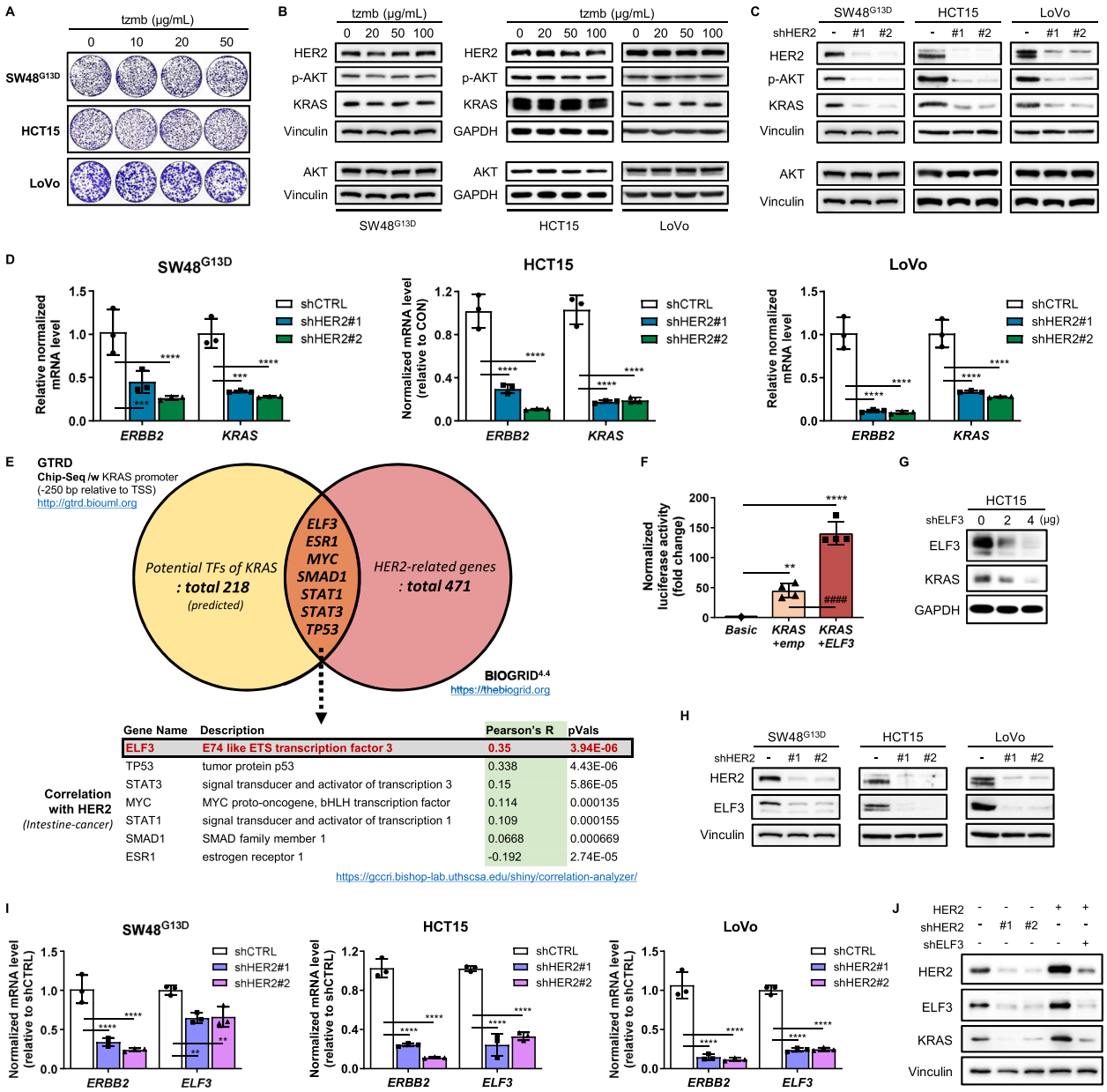

Fig. 5 Transcriptional regulatory axis of HER2-ELF3-KRAS as a therapeutic target for *KRAS*^{G13D} CRCs. **A**, **B** The anti-proliferative effect of trastuzumab (**A**) and its impact on HER signaling (**B**) were assessed in SW48^{G13D}, HCT15, and LoVo cells. Trastuzumab was applied for 10 days (**A**) and 16 h (**B**) at the indicated concentrations. **C**, **D** shHER2-mediated alteration in HER signaling (**C**) and *KRAS* mRNA levels (**D**) ($n = 3$, mean ± S.D, normalized to *GAPDH*) were investigated in SW48^{G13D}, HCT15 and LoVo cells. Cells were harvested after 36 h of incubation (ANOVA, $^{***}p < 0.001$, $^{****}p < 0.0001$, vs. shCTRL). **E** Schematic representation of the HER2-ELF3-KRAS transcriptional regulatory network. **F** Reporter gene assay was performed using pGL3-KRAS reporter gene. pGL3-KRAS was co-transfected with empty vector or pcDNA3.1-ELF3 for 24 h ($n = 4$, mean ± S.D). β-Gal was used for normalization of transfection efficiency (ANOVA, $^{**}p < 0.01$, $^{****}p < 0.0001$ vs. Basic, $^{\#\#\#\#}p < 0.0001$ vs. *KRAS* + *emp*). **G** shELF3-mediated changes in the KRAS expression level were evaluated after transient transduction for 24 h. **H**, **I** shHER2-induced alterations in protein (**H**) and gene (**I**) expression level of HER2 and ELF3 were assessed ($n = 3$, mean ± S.D, normalized to *GAPDH*). (ANOVA, $^{**}p < 0.01$, $^{****}p < 0.0001$ vs. shCTRL). **J** Changes in KRAS expression levels were evaluated in SW48^{G13D} cells following pCDH-HER2 overexpression, shHER2 knockdown, and shELF3 transduction. HER2 overexpression and knockdown were stably induced, while shELF3 was transiently transfected for 24 h

common between the two datasets. To prioritize genes that have higher chance to be co-regulated with HER2, we assessed the co-expression correlation between HER2 and each of the seven identified TFs using Correlation AnalyzeR [42, 43]. Among these, ELF3 displayed the highest correlation value (Pearson's R), signifying a

statistically significant association with HER2 (Fig. 5E). Leveraging Transcription Factor Binding Site (TFBS) analysis, we conducted a luciferase promoter assay, which clearly demonstrated that ELF3 activates the *KRAS* promoter. This was evidenced by a substantial increase in KRAS promoter activity following co-transfection with ELF3 (Fig. 5F). Additionally, knockdown of ELF3 resulted in a notable decrease in KRAS levels (Fig. 5G), strongly supporting the role of ELF3 as a direct TF governing KRAS expression.

ELF3 is a well-established transcription factor for HER2, functioning through its interaction with the transcriptional coactivator, MED23. Conversely, ELF3 has also been identified as one of the HER2-activated genes, establishing a bidirectional regulatory relationship. Ectopic expression of HER2 has been shown to directly increase the ELF3 promoter activity, primarily through the PI3K/AKT pathway [27, 44]. Our investigation revealed that ELF3 was notably depleted along with HER2 knockdown (Fig. 5H), specifically, at the mRNA level (Fig. 5I), and was not associated with proteasomal degradation (Supplementary Fig. 5B). Consistent with findings so far, HER2 overexpression induced upregulation of ELF3, which in turn elevated KRAS levels. However, in the absence of ELF3, HER2 overexpression failed to induce such effects, confirming that HER2-induced KRAS upregulation is predominantly mediated through ELF3 (Fig. 5J).

HER3-driven specificity of HER2-ELF3-KRAS axis for *KRAS*^{G13D}CRC

To gain deeper insight into the transcriptional landscape underlying the HER2-ELF3-KRAS axis across different *KRAS* mutation contexts, we generated RNA-seq profiles from control and HER2-silenced SW48 (HER2^{high}) isogenic cell lines. HER2 knockdown consistently reduced *ELF3* mRNA levels across *KRAS*^{WT}, *KRAS*^{G12V}, and *KRAS*^{G13D} backgrounds, suggesting that HER2-ELF3 transcriptional regulation is not exclusive to the *KRAS*^{G13D} context. However, the magnitude of *ELF3* suppression was markedly greater in *KRAS*^{G13D} cells, and a significant reduction in KRAS mRNA levels was observed only in this background (Supplementary Fig. 5D). These transcriptional changes were mirrored at the protein level: HER2 knockdown led to a marked reduction in both ELF3 and KRAS proteins, but again, only in *KRAS*^{G13D} cells (Supplementary Fig. 5E). In line with these findings, only CRC cell lines harboring the *KRAS*^{G13D} mutation showed a positive correlation between the expression patterns of HER2, ELF3 and KRAS (Supplementary Fig. 5F), further supporting the *KRAS*^{G13D}-specific nature of the HER2-ELF3-KRAS regulatory axis. Consistently, analysis of the GSE39582 dataset revealed that HER2 and KRAS mRNA levels were most strongly correlated in *KRAS*^{G13D} CRC patients, compared to those with *KRAS*^{WT} or *KRAS*^{G12} variants (Supplementary Fig. 5G). GSEA showed that the Hallmark_KRAS_Signaling_Up gene set—comprising genes upregulated by KRAS activation—was positively enriched only in HER2^{high} *KRAS*^{G13D} patients (Supplementary Fig. 5H), suggesting selectively enhanced KRAS activity in this context.

Interestingly, further GSEA on the hallmark gene set collection revealed that the EMT pathway was the most significantly enriched pathway in ELF3^{high} *KRAS*^{G13D} CRCs, closely mirroring the enrichment observed in HER2^{high} *KRAS*^{G13D} CRC patients (Supplementary Fig. 5I, upper panel). Notably, over 80% of the top enriched genes overlapped between the HER2^{high} and ELF3^{high} *KRAS*^{G13D} CRCs (Supplementary Tables 2 and 5), indicating a strong convergence in their pathway enrichment profiles. In contrast, EMT was negatively enriched in ELF3^{high} *KRAS*^{G12} CRCs (Supplementary Fig. 5I, lower panel), highlighting that the HER2-ELF3-KRAS axis specifically regulates EMT in *KRAS*^{G13D} CRCs and may underlie driving their aggressive phenotype.

To investigate the molecular basis underlying the *KRAS*^{G13D}-specific activation of the HER2–ELF3–KRAS axis, we explored whether differential dimerization patterns of HER2 with other HER family members could explain this specificity. As an orphan receptor, HER2 requires dimerization with other HER family members to effectively activate downstream signaling [45]. We therefore analyzed the expression of HER1, HER3, and HER4 across CRC cell lines and assessed the impact of HER2 knockdown on the expression of these receptors and their associated signaling pathways. Our analysis on 56 CRC cell lines from the CCLE database revealed that *KRAS*^{G13D} mutant cells tend to express lower HER3 expression and higher HER1 levels, compared to *KRAS*^{WT} or *KRAS*^{G12} mutant cells (Supplementary Fig. 6A). HER4 expression was consistently low across all cell lines, and undetectable in our experimental system (Supplementary Fig. 6A, B). Despite lower basal HER3 expression in *KRAS*^{G13D} cells, our comparison of isogenic SW48 cell lines harboring different *KRAS* mutation subtypes revealed that HER2 silencing led to a notable downregulation of HER3 specifically in SW48^{G13D} cells, along with a significant reduction in p-AKT and p-MAPK levels (Supplementary Fig. 6B). In contrast, HER1 expression and its downstream signaling (p-AKT and p-MAPK) remained largely unchanged in *KRAS*^{WT} or *KRAS*^{G12} mutant cells.

Unlike HER1 and HER4, which possess intrinsic kinase activity and can activate downstream pathway through homo- or heterodimerization with HER2, HER3 lacks such intrinsic kinase activity and depends entirely on

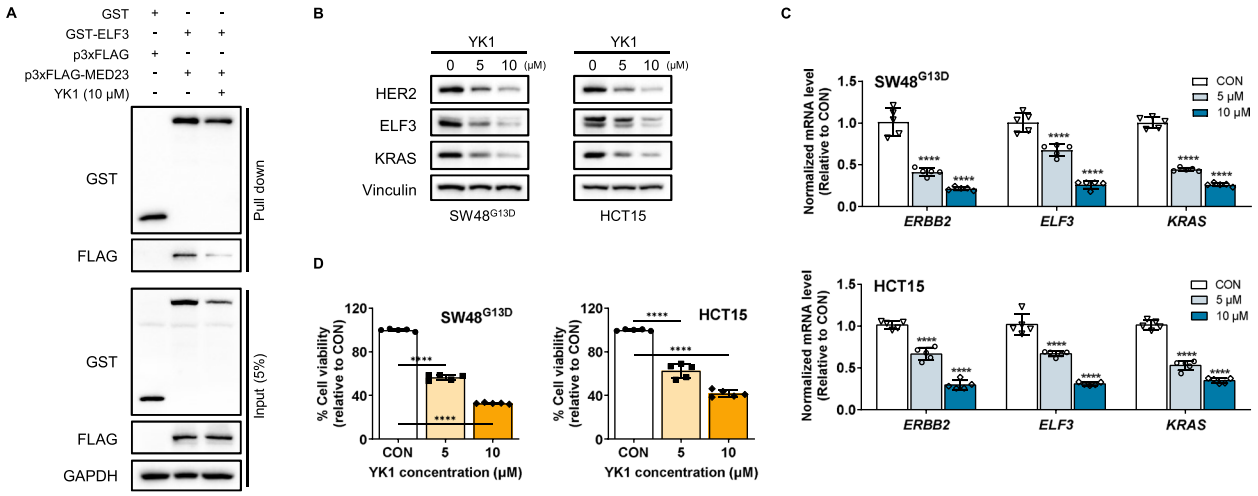

Fig. 6 Inhibition of ELF3-MED23 as a novel therapeutic approach to attenuate the HER2-ELF3-KRAS axis in *KRAS*^{G13D} CRCs. **A** GST pull-down assay was performed using GST-ELF3. GST-ELF3 was co-transduced with either empty p3xFLAG or p3xFLAG-ELF3 construct. YK1 was applied 12 h post-transfection and maintained for additional 12 h prior to cell harvest. **B**, **C** YK1-mediated alterations in protein (**B**) and gene (**C**) expression levels of HER2, ELF3, and KRAS were evaluated ($n = 5$, mean ± S.D, normalized to *GAPDH*). (ANOVA, $^{****}p < 0.0001$ vs. CON). **D** The growth inhibitory effect of YK1 was assessed in SW48^{G13D} and HCT15 cells. YK1 was treated for 48 h at the indicated concentrations ($n = 5$) (ANOVA, $^{****}p < 0.0001$ vs. CON)

dimerization with HER2 for downstream signaling activation [46]. HER2-HER3 dimerization is known to strongly activate the PI3K/AKT pathway, though it also contributes to the MAPK/ERK pathway activation, albeit to a lesser extent [47, 48]. Reflecting these distinct signaling capacities, *KRAS*^{WT} and *KRAS*^{G12} mutant cells showed sustained expression of other HER family proteins and preserved downstream signaling activity (Supplementary Fig. 6B), suggesting that they predominantly rely on HER1 homodimers rather than HER2-dependent signaling. This likely explains their minimal response to HER2 knockdown. In contrast, *KRAS*^{G13D} cells showed strong suppression of both PI3K/AKT and MAPK pathways following HER2 knockdown, indicating a specific dependency on HER2-mediated signaling, particularly through HER2–HER3 dimerization.

Moreover, we found that NRG1, a key ligand that activates HER3 and facilitates HER2-HER3 interactions [49], was significantly upregulated in *KRAS*^{G13D} cells compared to other *KRAS* subtypes (Supplementary Fig. 6C). Notably, NRG1 expression was markedly reduced upon HER2 silencing, again only in the *KRAS*^{G13D} background (Supplementary Fig. 6D). This distinct molecular profile further supports the idea that *KRAS*^{G13D} cells preferentially rely on HER2-HER3 dimer-driven signaling for their survival. In further support of the *KRAS*^{G13D}-specific HER2-HER3 dependence, GSEA of both our RNA-seq data and GSE39582 dataset revealed strong positive enrichment of the PI3K/AKT signaling pathway signature in HER2^{high} *KRAS*^{G13D} cases, with notably elevated NES values (Supplementary Fig. 6E, F). Importantly, in the GSE39582 cohort, HER2^{high} *KRAS*^{WT} and *KRAS*^{G12} variants CRCs even exhibited negative NES values (Supplementary Fig. 6F), further underscoring the *KRAS*^{G13D}-specific activation of this pathway. Consistently, GSEA of RNA-seq data confirmed that the HER2-HER3 pathway signature was positively enriched in *KRAS*^{G13D} CRC cells, showing the highest NES value among CRC cell lines with different KRAS statuses (Supplementary Fig. 6G). Given that PI3K/AKT signaling regulates ELF3 expression, these findings support a model in which HER2–HER3-mediated PI3K/AKT activity uniquely sustains the ELF3–KRAS transcriptional program in *KRAS*^{G13D} cells.

Taken together, although the HER2–ELF3 interaction may be broadly present across CRCs, functional activation of the HER2–ELF3–KRAS axis occurs to a biologically meaningful extent only in *KRAS*^{G13D} CRCs, driven by their preferential dependence toward HER2-HER3 dimerization. This highlights the biological and therapeutic specificity of this regulatory network in the *KRAS*^{G13D} context.

Inhibition of the ELF3-MED23 interaction as a novel therapeutic approach to attenuate the HER2-ELF3-KRAS axis in *KRAS*^{G13D} mutant CRCs

ELF3 functions in collaboration with the specific coactivator MED23, a Ras-linked subunit of the human mediator complex, to facilitate the transcription of HER2 [27, 50]. To transcriptionally downregulate HER2, we devised a strategy to selectively disrupt the ELF3-MED23 protein–protein interaction (PPI), which is specific to HER2 regulation. We evaluated this approach as a potential

therapeutic strategy for treating $KRAS^{G13D}$ CRCs. To achieve this, we used a synthetic pyrazoline analog, YK1, developed by our group as a potent and selective PPI inhibitor for ELF3-MED23 [27]. Through a GST-pull down assay, we initially confirmed the efficacy of YK1 in inhibiting the ELF3-MED23 interaction in $KRAS^{G13D}$ CRC cells (Fig. 6A). Following this inhibition, YK1 successfully induced transcriptional downregulation of HER2, concurrently leading to the depletion of ELF3 and KRAS at the mRNA level (Fig. 6B, C). This, in turn, resulted in significant growth inhibition of the tested cell lines (Fig. 6D).

Transcriptional downregulation of HER2 through YK1 as a strategy to overcome therapeutic limitations of $KRAS^{G13D}$ CRC cells

Further assessments involving the co-treatment of YK1 with CTX revealed varying effects of YK1-mediated HER2 downregulation on CTX responsiveness across different *KRAS* mutation subtypes in SW48 isogenic cell lines (Fig. 7A-F). In $SW48^{WT}$ cells, YK1 treatment led to acquired resistance to CTX, as evidenced by a combination index (CI) value of 13.86, indicating significant antagonism between CTX and YK1 (Fig. 7A and E). Conversely, $SW48^{G12D}$ and $SW48^{G12V}$ cells were minimally affected by YK1, exhibiting non-significant changes in overall cell viability with CI values (1.07 and 1.21, respectively) which indicate slight antagonism (Fig. 7B, C, and E). Distinctively, the $SW48^{G13D}$ clone showed notable cell growth inhibition upon co-treatment with CTX and YK1 (Fig. 7D). In this subtype, a CI value of 0.22 indicated strong synergism (Fig. 7E), supporting the effectiveness of HER2 downregulation in restoring CTX sensitivity in $KRAS^{G13D}$ CRCs. These findings were further confirmed in $SW48^{G13D}$ and HCT15 ($KRAS^{G13D}$, $HER2^{high}$) cells, where long-term proliferation rates were significantly inhibited by both YK1 alone and the CTX + YK1 combination (Fig. 7F). We found that although YK1 treatment consistently downregulated HER2 expression, $KRAS^{WT}$ and $KRAS^{G12}$ variant cells did not exhibit changes in the expression of other HER family members (HER1 and HER3), nor in downstream signaling pathway, such as p-AKT (Supplementary Fig. 7A). Additionally, KRAS and ELF3 expression levels remained unchanged in these cell lines following YK1 treatment (Supplementary Fig. 7 A). In contrast, $KRAS^{G13D}$ cells exhibited a distinct and more sensitive response to HER2 suppression. YK1 treatment in these cells led to a marked reduction in HER3 and p-AKT levels, along with a notable reduction in both KRAS and ELF3 expression (Supplementary Fig. 7A), whereas CTX alone treatment did not induce any notable changes (Supplementary Fig. 7B). These effects were further enhanced by co-treatment with CTX, resulting in a synergistic anti-cancer response (Fig. 7E).

Additionally, YK1 treatment significantly attenuated the EMT process in $KRAS^{G13D}$ $HER2^{high}$ CRC cells, as indicated by the upregulation of epithelial markers and downregulation of mesenchymal markers (Fig. 7G). This was accompanied by a notable reduction in the migration potential of the tested cell lines (Fig. 7H), demonstrating the capability of YK1 to attenuate the oncogenic potential of $KRAS^{G13D}$ CRC cells through effective downregulation of HER2 expression. These results underscore the distinctive significance of targeting HER2 to overcome the therapeutic limitations of $KRAS^{G13D}$ CRCs.

Induction of significant anticancer effects by YK1 in $KRAS^{G13D}$ CRC tumors

To further evaluate the efficacy of YK1, we assessed its in vivo effects using a xenograft mouse model with the $SW48^{G13D}$ cell line. As expected, the tumors exhibited resistance to CTX; however, both co-administration and mono-administration of YK1 resulted in significant tumor growth inhibition. These findings underscore the significance of HER2 downregulation in $KRAS^{G13D}$ $HER2^{high}$ CRCs, and further support YK1's potential as a promising therapeutic option to overcome CTX resistance in these tumor subtypes (Fig. 8A-C). Subsequent immunohistochemistry (IHC) analysis revealed that the inhibitory effects on tumor growth were accompanied by a marked reduction in HER2 intensity and a decreased number of Ki67-positive cells in the tumor tissue treated with YK1 (Fig. 8D). The YK1-induced HER2 downregulation was confirmed at the transcriptional level, showing a remarkable decrease in the mRNA levels of *ERBB2*, *ELF3*, and *KRAS* (Fig. 8E). This indicates that the primary mechanism behind YK1-mediated anti-tumor activity lies in the attenuation of the HER2-ELF3-KRAS transcriptional regulatory network. As a result, there was a significant reversal of the EMT process, indicated by the upregulation of epithelial markers and downregulation of mesenchymal markers in tumor tissues (Fig. 8F). Significant anticancer effects of YK1 were further confirmed through an orthotopic CRC mouse model, collectively substantiating YK1 as a promising therapeutic intervention for overcoming CTX resistance and reversing the EMT process in $KRAS^{G13D}$ CRCs (Fig. 8G).

Discussion

Tumorigenesis of CRC is often characterized by the accumulation of mutations in various genes, including *KRAS*, *NRAS*, *BRAF*, *PIK3CA*, and *PTEN* [51]. Among these, *KRAS* mutations are the most prevalent, occurring in 30–40% of CRC cases, leading to persistent activation of downstream signaling pathways. Consequently,

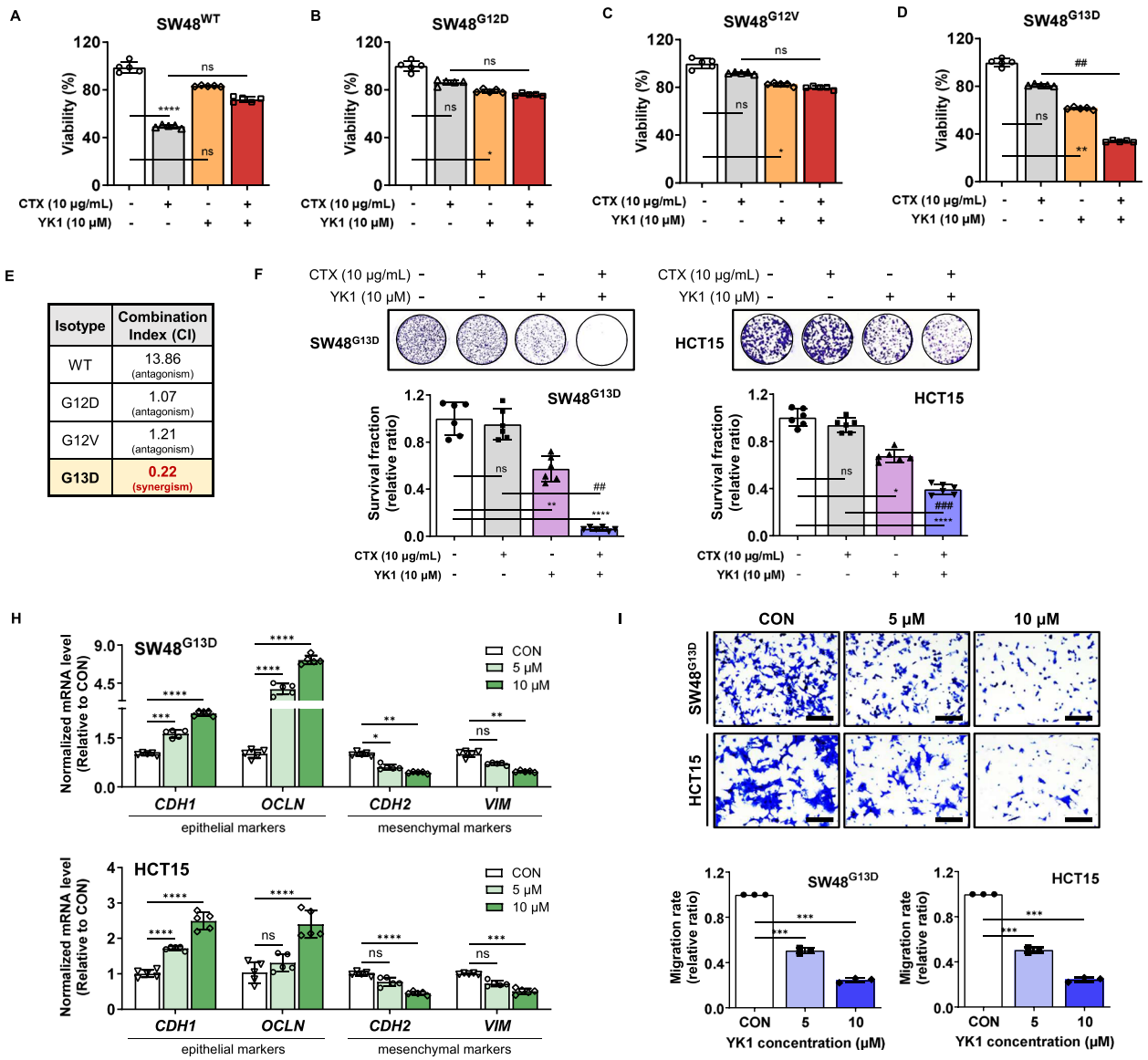

Fig. 7 Transcriptionally downregulating HER2 via YK1 as a relevant strategy to overcome therapeutic limitations of *KRAS*^{G13D} CRC cells. **A-D** The effect of YK1 and CTX co-treatment on cell viability was assessed on SW48 isogenic cell lines [SW48^{WT} (**A**), SW48^{G12D} (**B**), SW48^{G12V} (**C**), and SW48^{G13D} (**D**)]. Cells were treated with the indicated concentrations for 24 h (ANOVA, ns = non-significant, $^{**}p < 0.0001$, $^{****}p < 0.0001$ vs. control, $^{\#\#}p < 0.0001$ vs. CTX). **E** Combination index (CI) values for YK1 (10 μM) and CTX (10 μg/mL) in SW48 isogenic cell lines were calculated using Compusyn software. **F** Co-treatment effects of YK1 and CTX on colony-forming ability were measured against SW48^{G13D} and HCT15 cells ($n = 5$) following a 10 d-incubation at indicated concentrations (ANOVA, ns = non-significant, $^{*}p < 0.05$, $^{**}p < 0.01$, $^{****}p < 0.0001$ vs. control (0), $^{\#\#}p < 0.01$, $^{\#\#\#}p < 0.01$ vs. CTX). **G** YK1-induced changes in EMT marker gene expression were examined in SW48^{G13D} and HCT15 cells after 16 h of treatment at the indicated concentrations ($n = 5$, mean ± S.D., normalized to GAPDH) (ANOVA, ns = non-significant, $^{***}p < 0.001$, $^{****}p < 0.0001$ vs. CON). **H** Transwell migration assay was performed after 16 h of YK1 treatment in SW48^{G13D} and HCT15 cells at the indicated concentrations. Images were captured at 200 × magnification (scale bars = 100 μm). Quantification of cell migration was conducted using ImageJ software, presented as a relative ratio on CON ($n = 3$). (ANOVA, $^{***}p < 0.001$ vs. CON)

mutated *KRAS* has been suggested as a major oncogenic driving factor and a reliable negative biomarker for predicting the efficacy of anti-EGFR agents in CRCs. Despite being considered"undruggable"for decades due to its small and shallow surface, recent developments of irreversible covalent inhibitors for *KRAS*^{G12C}, like AMG510 (Sotorasib) and MRTX849 (Adagrasib), have shown promising clinical outcomes, making mutant *KRAS* a"druggable"target [52–55]. These advances have fostered hope for developing specific inhibitors for each

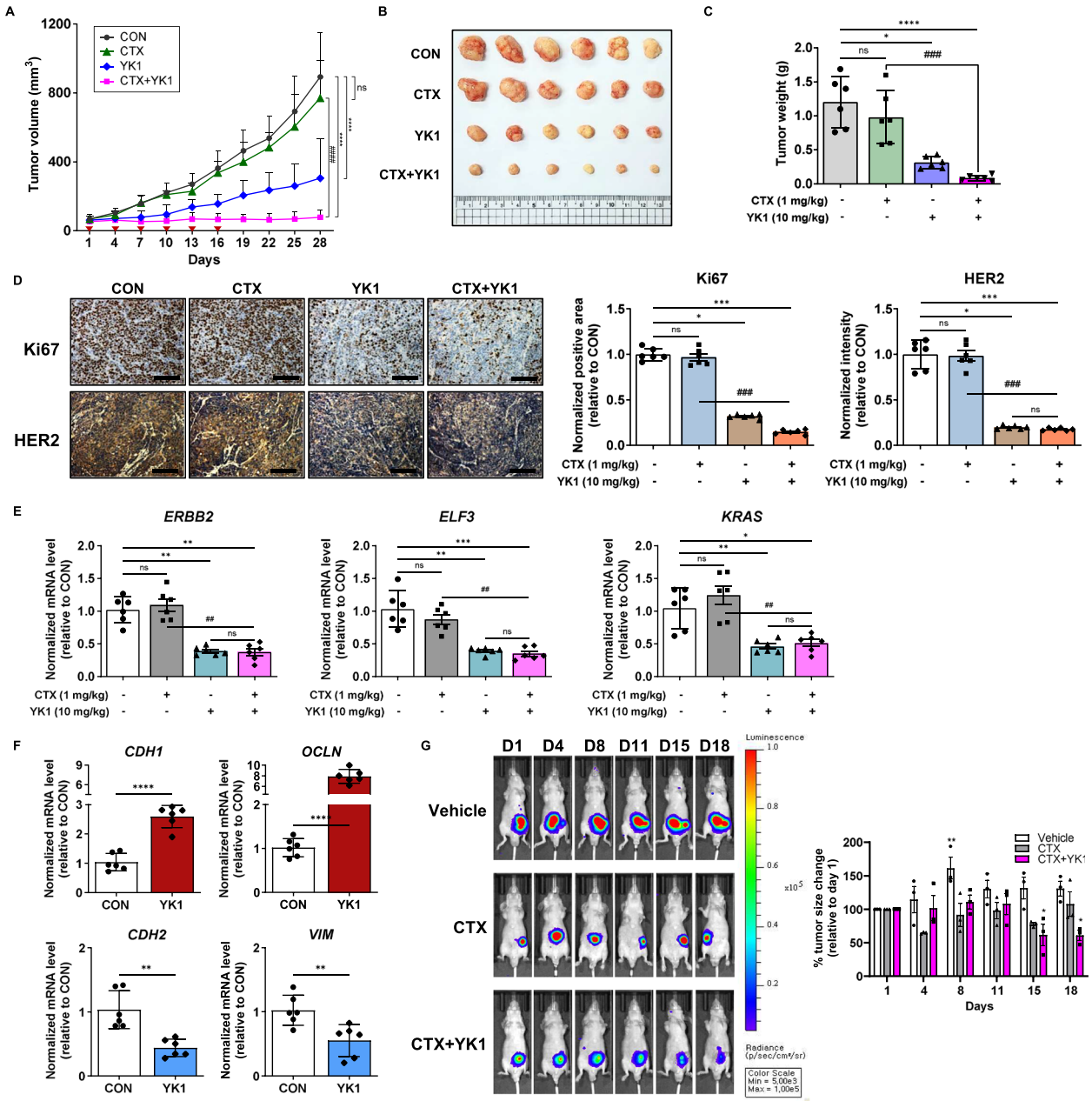

Fig. 8 YK1 induces potent anti-cancer effects in *KRAS*^{G13D} CRC tumors. **A** The co-administration effect of CTX (1 mg/kg) and YK1 (10 mg/kg) was evaluated in an in vivo xenograft mouse model using SW48^{G13D} cells ($n = 6$). Drug administration began on day 1, and tumor length and width were measured with calipers. Tumor volumes were calculated using the formula: (length × width^2)/2. Data are presented as mean ± S.E.M. (ANOVA, ns = non-significant, $^{****}p < 0.0001$ vs. CON, $^{\#\#\#\#}p < 0.0001$ vs. CTX). **B** Representative images of the excised tumors from each group ($n = 6$). **C** Tumor weights were assessed across treatment groups ($n = 6$). (ANOVA, ns = non-significant, $^{*}p < 0.05$, $^{****}p < 0.0001$ vs. CON, $^{\#\#\#}p < 0.001$ vs. CTX). **D** IHC staining for Ki67 and HER2 was performed on tumor tissues from each group. The positive area and intensity (both normalized to CON) were quantified for Ki67 and HER2, respectively ($n = 6$, 10 independent fields per animal). Data are shown as mean ± S.D. (ANOVA, ns = non-significant, $^{*}p < 0.05$, $^{**}p < 0.01$, $^{***}p < 0.001$ vs. CON, $^{\#\#\#}p < 0.001$ vs. CTX). **E**, **F** Gene expression levels of HER2, ELF3, KRAS (**E**), and EMT markers (**F**) were evaluated in tumor tissues from the indicated treatment groups ($n = 6$, mean ± S.D, normalized to *GAPDH*). (ANOVA, ns = non-significant, $^{*}p < 0.05$, $^{**}p < 0.01$, $^{***}p < 0.001$ vs. CON, $^{\#\#}p < 0.001$ vs. CTX). **G** The combined effect of CTX (1 mg/kg) and YK1 (20 mg/kg) was tested in an in vivo orthotopic mouse model of HCT15-luc cells ($n = 3$). Tumor growth was monitored for 18 days using bioluminescent imaging. Data are presented as the percentage change in tumor size relative to day 1 (mean ± S.E.M.). (ANOVA, $^{*}p < 0.05$, $^{**}p < 0.01$ vs. Vehicle on day 1)

KRAS mutation subtype to improve precision medicine and therapeutic outcomes. Sotorasib and Adagrasib have been FDA-approved for the treatment of metastatic or locally advanced non-small cell lung cancer (NSCLC), where $KRAS^{G12C}$ is the most common variant, accounting for approximately 40% of *KRAS* mutations and found in 10–13% of all NSCLC cases [55]. In CRCs, the most *KRAS* mutations are G12D, G12V, and G13D [56]. While a non-covalent and selective inhibitor of $KRAS^{G12D}$, MRTX1133, is currently under a phase I/II clinical trials (NCT05737706), inhibitors targeting $KRAS^{G12V}$ and $KRAS^{G13D}$ remain in preclinical development [57]. Despite the association of $KRAS^{G13D}$ with a worse prognosis compared to other *KRAS* subtypes [29, 58, 59], there are minimal studies proposing effective therapeutic strategies for $KRAS^{G13D}$, and direct specific inhibitors for $KRAS^{G13D}$ are not yet available [60]. As part of a continuous effort to establish effective mutation-selective inhibitory approaches for KRAS, multiple studies have highlighted isoform-dependent differences in the function and oncogenic potentials of *KRAS* mutations [61–63]. These investigations reveal that individual *KRAS* mutants can lead to distinct biological and clinical outcomes by activating different signaling pathways [64, 65].

In this study we focused on unraveling the unique biological behaviors exhibited by $KRAS^{G13D}$ mutants, noting that $KRAS^{G13D}$ CRC patients typically experience a poorer prognosis compared to those with other *KRAS* mutant subtypes. However, some $KRAS^{G13D}$ CRC patients can still derive clinical benefits from anti-EGFR drugs, particularly CTX. *KRAS* mutations generally lead to the constitutive activation of downstream signaling cascades, such as MAPK and AKT pathways, which typically render CTX ineffective. Nevertheless, given the observed responsiveness of some $KRAS^{G13D}$ CRC patients to CTX [10], we hypothesized that a crucial determinant for CTX sensitivity in $KRAS^{G13D}$ CRCs might be located upstream of KRAS. This led us to focus on HER2 and explore its potential prognostic and predictive value in $KRAS^{G13D}$ CRCs.

While the association of HER2 amplification/overexpression with anti-EGFR resistance in CRCs as a negative predictive biomarker is well-established, its prognostic role remains controversial. Nonetheless, various preclinical and clinical trials have demonstrated the considerable efficacy and tolerable safety profile of anti-HER2 drugs, making HER2 a prominent actionable therapeutic target in CRCs. HER2 amplification/overexpression is found in approximately 3% of CRC patients, with a higher prevalence reported in *RAS/BRAF* wild-type tumors, ranging from 5 to 14%. Consequently, according to NCCN guidelines, HER2-targeted therapy is now recommended as subsequent therapy options for *RAS* wild-type, *BRAF* wild-type, and *HER2* amplified CRC patients [14, 26]. However, few studies have examined the significance of HER2 amplification/overexpression in the context of *KRAS* mutations, and none have considered the impact of each *KRAS* mutation subtype independently. Our study is the first to investigate the role of HER2 across different *KRAS* mutation statuses in CRCs, underscoring the originality and novelty of our research.

We have comprehensively analyzed the clinical significance of HER2 across different *KRAS* mutation subtypes and clarified HER2 as a crucial therapeutic target specifically for $KRAS^{G13D}$ CRCs (Figs. 1, 2 and 3). In line with this mutation specificity, we uncovered a novel transcriptional regulatory network, the HER2-ELF3-KRAS axis, in which ELF3 serves as a shared transcription factor for both *HER2* and *KRAS* genes (Fig. 5). Importantly, our additional RNA-seq and functional analyses revealed that this axis is preferentially activated in $KRAS^{G13D}$ CRC cells. HER2 knockdown led to a significant reduction in ELF3 and KRAS expression specifically in the $KRAS^{G13D}$ background, correlating with enhanced KRAS signaling and EMT pathway enrichment. This specificity is mechanistically attributed to the dependency of $KRAS^{G13D}$ cells on HER2–HER3 dimerization, which strongly activates the PI3K/AKT pathway, thereby sustaining ELF3-mediated transcriptional regulation. Moreover, we found that elevated expression of NRG1 in $KRAS^{G13D}$ cells further promotes HER2–HER3 interaction, reinforcing this signaling axis (Supplementary Figs. 5–6). Through extensive analysis of publicly available databases, we demonstrated that the HER2–ELF3–KRAS axis is selectively activated in $KRAS^{G13D}$ CRCs (Fig. 5, Supplementary Fig. 5E-H), highlighting its specific pro-oncogenic role in promoting the EMT process (Fig. 4, Supplementary Fig. 5I). These findings emphasize the therapeutic relevance of targeting the HER2-ELF3-KRAS network, particularly in $KRAS^{G13D}$ CRCs. ELF3 may not display mutation-specific transcriptional activity based on *KRAS* subtypes; therefore, the HER2-ELF3-KRAS axis could represent a universal axis across various cancer types, irrespective of their *KRAS* mutations status. However, inhibiting this axis – either through silencing HER2 or ELF3 (Fig. 5J) or through pharmacological disruption of the ELF3-MED23 interaction (Figs. 7 and 8) – restores CTX sensitivity specifically in $KRAS^{G13D}$ CRCs. This suggests that while the HER2-ELF3-KRAS network may have broad applicability, its functional significance and therapeutic relevance vary depending on the molecular context. Thus, the effectiveness of targeting this axis as a therapeutic strategy depends on factors such as *KRAS* mutation status and the expression levels of ELF3, HER2, and KRAS.

This context-specific variability is particularly evident when comparing $KRAS^{G13D}$ and $KRAS^{G12}$ mutations.

$KRAS^{G13D}$ cancers retain some regulatory capabilities similar to $KRAS^{WT}$ cancers due to their intermediate sensitivity to NF1 (neurofibromin)-mediated GTP hydrolysis, unlike $KRAS^{G12}$ mutations, which are largely insensitive to this process [9]. As a result, KRAS protein levels may play critical role in promoting tumor aggressiveness in $KRAS^{G13D}$ cancers, where high KRAS abundance could potentially overwhelm the partial regulatory capabilities of NF1, leading to persistent oncogenic signaling. In contrast, $KRAS^{G12}$ mutations, which exhibit nearly complete impairment of GAP-mediated hydrolysis, maintain a constitutively active state, making cancer aggressiveness more dependent on KRAS activity itself rather than on protein levels. Further research is needed to elucidate the underlying mechanisms.

Based on our findings, we introduced YK1, a small molecule inhibitor that disrupts the ELF3-MED23 interaction, leading to the transcriptional downregulation of HER2 and KRAS. This intervention significantly attenuated the HER2-ELF3-KRAS axis, potentially reducing the hyperactivated cell signaling system to its normal status. As a result, $KRAS^{G13D}$ CRCs were sensitized to CTX (Figs. 7D-F and 8A-E), and their tumorigenic potential was reduced by inhibiting the EMT process (Figs. 7G, H and 8F, G).

A key advantage of targeting the ELF3-MED23 interaction, rather than directly inhibiting ELF3 or KRAS, is the selective downregulation of HER2, which minimizes the risk of unintended side effects associated with the broader involvement of ELF3 and KRAS in diverse signaling cascades [52, 66]. This approach allows for the selective regulation of the HER2-ELF3-KRAS axis with a reduced likelihood of affecting unintended pathways, overall leading to significant anticancer activity in $KRAS^{G13D}$ CRCs.

Previous attempts to reduce KRAS expression using antisense oligonucleotides (ASOs; AZX4785) were unsuccessful in achieving positive clinical outcomes [52, 66]. Our approach holds greater potential as it simultaneously suppresses HER2 and KRAS expression, thereby addressing alternative signaling pathways that may be activated as compensatory responses to KRAS downregulation.

Conclusion

This study highlights the critical role of HER2 as a key determinant in the unique biological characteristics of $KRAS^{G13D}$ CRCs. Our investigations revealed a strong association between HER2 overexpression and lower survival rates, increased aggressiveness, and resistance to CTX, particularly in $KRAS^{G13D}$ CRCs. We identified a novel transcriptional regulatory network involving HER2, ELF3, and KRAS, where ELF3 acts as a key TF regulating KRAS expression in the context of HER2 overexpression. We propose this HER2-ELF3-KRAS axis as a potential therapeutic target for $KRAS^{G13D}$ CRCs and have thoroughly demonstrated the relevance and effectiveness of its regulation.

Based on these findings, we successfully identified YK1, a novel small molecule capable of disrupting this network, and demonstrated its potential as a targeted intervention specifically effective for $KRAS^{G13D}$ CRCS. The significance of this study lies not only in identifying a new target but also in presenting a specific pharmacological approach for regulating this network, confirming the feasibility of modulating this axis. We believe that the groundbreaking findings from this study hold the potential to open new avenues for developing tailored interventions for $KRAS^{G13D}$ CRCs, offering valuable insights into the ongoing efforts in the pursuit of realizing precision medicine for CRCs.

Supplementary Information

The online version contains supplementary material available at https://doi.org/10.1186/s12943-025-02343-5.

Supplementary Material 1.

Supplementary Material 2.

Acknowledgements

The authors thank the Ewha Drug Development Research Core Center for assistance with analyses using NMR, UV/vis spectrophotometry, Apotome laser scanning microscope, microplate reader, Chemidoc, and IVIS instruments.

Authors' contributions

S.-Y.H. designed the project, conducted experiments, acquired data, analyzed data, and wrote the manuscript, Y.S. conducted experiments with patient samples and analyzed related data, S.P. designed some experiments, conducted experiments, and acquired data, S.-A.K., S.K., E.S.P., I.M., Y.L., S.J, H.K., I.S. conducted several animal experiments, and acquired data, K.-H.J. M.A. conducted some experiments, Y.N. designed and synthesized small molecules, T.K. provided patient samples and reviewed the data, H.L., S.-Y.P, reviewed data and manuscript, Y.K. designed the research project, reviewed data, and wrote the manuscript.

Funding

This work was supported by grants from the National Research Foundation of Korea (NRF), funded by the Korean government (MSIT) (NRF-2022R1 A2 C2092053 and RS-2024-00431505). The authors thank the Ewha Drug Development Research Core Center for assistance with analyses using NMR, UV/vis spectrophotometry, Apotome laser scanning microscope, microplate reader, Chemidoc, and IVIS instruments.

Data availability

No datasets were generated or analysed during the current study.

Declarations

Ethics approval and consent to participate

All animal experiments were approved by the Institutional Animal Care and Use Committee (IACUC) at Ewha Womans University. All studies involving human subjects were approved by the Institutional Review Board (IRB) of Severance Hospital of the Yonsei University (Seoul, Korea) (IRB#4–2012-0859).

Written informed consent was obtained from all patients prior to sample collection.

Consent for publication
Not applicable.

Competing interests
The authors declare no competing interests.

Author details
[1]College of Pharmacy, Graduate School of Pharmaceutical Sciences, Ewha Womans University, Seoul 03760, Republic of Korea. [2]Graduate Program in Innovative Biomaterials Convergence, Ewha Womans University, Seoul 03760, Republic of Korea. [3]Division of Gastroenterology, Department of Internal Medicine, Yonsei University College of Medicine, 50 Yonseiro, Seodaemun-Gu, Seoul 03722, Republic of Korea. [4]BK21 FOUR Intelligence Computing, Seoul National University, Seoul, Republic of Korea. [5]Center for Genome Engineering, Institute for Basic Science, 55, Expo-Ro, Yuseong-Gu, Daejeon 34126, Republic of Korea. [6]College of Pharmacy, CHA University, Pocheon 11160, Republic of Korea.

Received: 19 October 2024 Accepted: 25 April 2025
Published online: 09 May 2025

References

1. Bray F, Ren JS, Masuyer E, Ferlay J. Global estimates of cancer prevalence for 27 sites in the adult population in 2008. Int J Cancer. 2013;132:1133–45.
2. Edwards BK, Ward E, Kohler BA, Eheman C, Zauber AG, Anderson RN, Jemal A, Schymura MJ, Lansdorp-Vogelaar I, Seeff LC, et al. Annual report to the nation on the status of cancer, 1975–2006, featuring colorectal cancer trends and impact of interventions (risk factors, screening, and treatment) to reduce future rates. Cancer. 2010;116:544–73.
3. Kruschewski M, Mueller K, Lipka S, Budczies J, Noske A, Buhr HJ, Elezkurtaj S. The Prognostic Impact of p53 Expression on Sporadic Colorectal Cancer Is Dependent on p21 Status. Cancers. 2011;3:1274–84.
4. Vogelstein B, Fearon ER, Hamilton SR, Kern SE, Preisinger AC, Leppert M, Nakamura Y, White R, Smits AM, Bos JL. Genetic alterations during colorectal-tumor development. N Engl J Med. 1988;319:525–32.
5. Dinu D, Dobre M, Panaitescu E, Birla R, Iosif C, Hoara P, Caragui A, Boeriu M, Constantinoiu S, Ardeleanu C. Prognostic significance of KRAS gene mutations in colorectal cancer–preliminary study. J Med Life. 2014;7:581–7.
6. Kim HS, Heo JS, Lee J, Lee JY, Lee MY, Lim SH, Lee WY, Kim SH, Park YA, Cho YB, et al. The impact of KRAS mutations on prognosis in surgically resected colorectal cancer patients with liver and lung metastases: a retrospective analysis. BMC Cancer. 2016;16:120.
7. Er TK, Chen CC, Bujanda L, Herreros-Villanueva M. Clinical relevance of KRAS mutations in codon 13: Where are we? Cancer Lett. 2014;343:1–5.
8. Uprety D, Adjei AA. KRAS: From undruggable to a druggable Cancer Target. Cancer Treat Rev. 2020;89: 102070.
9. Rabara D, Tran TH, Dharmaiah S, Stephens RM, McCormick F, Simanshu DK, Holderfield M. KRAS G13D sensitivity to neurofibromin-mediated GTP hydrolysis. Proc Natl Acad Sci U S A. 2019;116:22122–31.
10. Morelli MP, Kopetz S. Hurdles and Complexities of Codon 13 KRAS Mutations. J Clin Oncol. 2012;30:3565–7.
11. McFall T, Schomburg NK, Rossman KL, Stites EC. Discernment between candidate mechanisms for KRAS G13D colorectal cancer sensitivity to EGFR inhibitors. Cell Communication and Signaling. 2020;18:179.
12. Samowitz WS, Curtin K, Schaffer D, Robertson M, Leppert M, Slattery ML. Relationship of Ki-ras mutations in colon cancers to tumor location, stage, and survival: a population-based study. Cancer Epidemiol Biomarkers Prev. 2000;9:1193–7.
13. Kocian P, Sedivcova M, Drgac J, Cerna K, Hoch J, Kodet R, Bartunkova J, Spisek R, Fialova A. Tumor-infiltrating lymphocytes and dendritic cells in human colorectal cancer: their relationship to KRAS mutational status and disease recurrence. Hum Immunol. 2011;72:1022–8.
14. Ahcene Djaballah S, Daniel F, Milani A, Ricagno G, Lonardi S. HER2 in colorectal cancer: the long and winding road from negative predictive factor to positive actionable target. Am Soc Clin Oncol Educ Book. 2022;42:1–14. https://doi.org/10.1200/EDBK_351354.
15. Suwaidan AA, Lau DK, Chau I. HER2 targeted therapy in colorectal cancer: New horizons. Cancer Treat Rev. 2022;105: 102363.
16. Gaye E, Penel N, Lebellec L. Novel treatment approaches for HER2 positive solid tumors (excluding breast cancer). Curr Opin Oncol. 2022;34:570–4.
17. Ivanova M, Venetis K, Guerini-Rocco E, Bottiglieri L, Mastropasqua MG, Garrone O, Fusco N, Ghidini M. HER2 in metastatic colorectal cancer: pathology, somatic alterations, and perspectives for novel therapeutic schemes. Life (Basel). 2022;12(9):1403. https://doi.org/10.3390/life12091403.
18. Moasser MM. The oncogene HER2: its signaling and transforming functions and its role in human cancer pathogenesis. Oncogene. 2007;26(45):6469–87. https://doi.org/10.1038/sj.onc.1210477. Epub 2007 Apr 30. PMID: 17471238; PMCID: PMC3021475.
19. Vranić S, Bešlija S, Gatalica Z. Targeting HER2 expression in cancer: new drugs and new indications. Bosn J Basic Med Sci. 2021;21(1):1–4. https://doi.org/10.17305/bjbms.2020.4908. PMID: 32530388; PMCID: PMC7861626.
20. Wang H, Miao J, Wen Y, Xia X, Chen Y, Huang M, Chen S, Zhao Z, Zhang Y, Chen C, Zhu X. Molecular landscape of ERBB2 alterations in 14,956 solid tumors. Pathol Oncol Res. 2022;28:1610360. https://doi.org/10.3389/pore.2022.1610360. PMID: 35911441; PMCID: PMC9325965.
21. Roy-Chowdhuri S, Davies KD, Ritterhouse LL, Snow AN. ERBB2 (HER2) alterations in colorectal cancer. J Mol Diagn. 2022;24(10):1064–6. https://doi.org/10.1016/j.jmoldx.2022.07.001. Epub 2022 Aug 7. PMID: 35944596.
22. Kavuri SM, Jain N, Galimi F, Cottino F, Leto SM, Migliardi G, Searleman AC, Shen W, Monsey J, Trusolino L, Jacobs SA, Bertotti A, Bose R. HER2 activating mutations are targets for colorectal cancer treatment. Cancer Discov. 2015;5(8):832–41. https://doi.org/10.1158/2159-8290.CD-14-1211. PMID: 26243863; PMCID: PMC4527087.
23. Afrăsânie VA, Marinca MV, Alexa-Stratulat T, Gafton B, Păduraru M, Adavidoaiei AM, Miron L, Rusu C. KRAS, NRAS, BRAF, HER2 and microsatellite instability in metastatic colorectal cancer - practical implications for the clinician. Radiol Oncol. 2019;53(3):265–74. https://doi.org/10.2478/raon-2019-0033. PMID: 31553708; PMCID: PMC6765160.
24. Ross JS, Fakih M, Ali SM, Elvin JA, Schrock AB, Suh J, Vergilio JA, Ramkissoon S, Severson E, Daniel S, et al. Targeting HER2 in colorectal cancer: The landscape of amplification and short variant mutations in ERBB2 and ERBB3. Cancer. 2018;124:1358–73.
25. Yonesaka K, Zejnullahu K, Okamoto I, Satoh T, Cappuzzo F, Souglakos J, Ercan D, Rogers A, Roncalli M, Takeda M, et al. Activation of ERBB2 signaling causes resistance to the EGFR-directed therapeutic antibody cetuximab. Sci Transl Med. 2011;3:99–ra86.
26. Benson AB, Venook AP, Al-Hawary MM, Arain MA, Chen Y-J, Ciombor KK, Cohen S, Cooper HS, Deming D. Farkas LJJotNCCN: Colon cancer, version 2.2021. NCCN Cli Pract Guid Oncolo. 2021;19:329–59.
27. Hwang SY, Park S, Jo H, Hee Seo S, Jeon KH, Kim S, Jung AR, Song C, Ahn M, Yeon Kwak S, et al. Interrupting specific hydrogen bonds between ELF3 and MED23 as an alternative drug resistance-free strategy for HER2-overexpressing cancers. J Adv Res. 2023;47:173–87.
28. Andreyev HJ, Norman AR, Cunningham D, Oates JR, Clarke PA. Kirsten ras mutations in patients with colorectal cancer: the multicenter "RASCAL" study. J Natl Cancer Inst. 1998;90:675–84.
29. Arrington AK, Heinrich EL, Lee W, Duldulao M, Patel S, Sanchez J, Garcia-Aguilar J, Kim J. Prognostic and predictive roles of KRAS mutation in colorectal cancer. Int J Mol Sci. 2012;13:12153–68.
30. Mao C, Huang YF, Yang ZY, Zheng DY, Chen JZ, Tang JL, Kras P. G13D mutation and codon 12 mutations are not created equal in predicting clinical outcomes of cetuximab in metastatic colorectal cancer: a systematic review and meta-analysis. Cancer. 2013;119:714–21.
31. Lee DW, Kim KJ, Han SW, Lee HJ, Rhee YY, Bae JM, Cho NY, Lee KH, Kim TY, Oh DY, et al. KRAS mutation is associated with worse prognosis in stage III or high-risk stage II colon cancer patients treated with adjuvant FOLFOX. Ann Surg Oncol. 2015;22:187–94.
32. Li J-L, Lin S-H, Chen H-Q, Liang L-S, Mo X-W, Lai H, Zhang J, Xu J, Gao B-Q, Feng Y, Lin Y. Clinical significance of HER2 and EGFR expression in colorectal cancer patients with ovarian metastasis. BMC Clin Pathol. 2019;19:3.

33. Saletti, Piercarlo, et al. EGFR signaling in colorectal cancer: a clinical perspective. Gastrointestinal Cancer: Targets and Therapy. 2015:21–38.
34. Van Cutsem E, Lenz H-J, Köhne C-H, Heinemann V, Tejpar S, Melezínek I, Beier F, Stroh C. Rougier P. Van Krieken JHJJoco: Fluorouracil, leucovorin, and irinotecan plus cetuximab treatment and RAS mutations in colorectal cancer. 2015;33:692–700.
35. Saoudi González N, Ros J, Baraibar I, Salvà F, Rodríguez-Castells M, Alcaraz A, García A, Tabernero J, Élez E. Cetuximab as a Key Partner in Personalized Targeted Therapy for Metastatic Colorectal Cancer. 2024;16:412.
36. Tejpar S, Bokemeyer C, Celik I, Schlichting M, Sartorius U, Van Cutsem E. Influence of KRAS G13D mutations on outcome in patients with metastatic colorectal cancer (mCRC) treated with first-line chemotherapy with or without cetuximab. J Clin Oncol. 2011;29(15):3511–3511.
37. Armaghany T, Wilson JD, Chu Q, Mills G. Genetic alterations in colorectal cancer. Gastrointest Cancer Res. 2012;5:19–27.
38. Cordo Russo RI, Chervo MF, Madera S, Charreau EH, Elizalde PV. Nuclear ErbB-2: a Novel Therapeutic Target in ErbB-2-Positive Breast Cancer? Horm Cancer. 2019;10:64–70.
39. Oughtred R, Rust J, Chang C, Breitkreutz BJ, Stark C, Willems A, Boucher L, Leung G, Kolas N, Zhang F, et al. The BioGRID database: A comprehensive biomedical resource of curated protein, genetic, and chemical interactions. Protein Sci. 2021;30:187–200.
40. Yevshin I, Sharipov R, Valeev T, Kel A, Kolpakov F. GTRD: a database of transcription factor binding sites identified by ChIP-seq experiments. Nucleic Acids Res. 2016;45:D61–7.
41. Yevshin I, Sharipov R, Kolmykov S, Kondrakhin Y, Kolpakov F. GTRD: a database on gene transcription regulation-2019 update. Nucleic Acids Res. 2019;47:D100-d105.
42. van Dam S, Võsa U, van der Graaf A, Franke L, de Magalhães JP. Gene co-expression analysis for functional classification and gene–disease predictions. Brief Bioinform. 2017;19:575–92.
43. Miller HE, Bishop AJR. Correlation AnalyzeR: functional predictions from gene co-expression correlations. BMC Bioinformatics. 2021;22:206.
44. Neve RM, Ylstra B, Chang C-H, Albertson DG, Benz CC. ErbB2 Activation of ESX gene expression. Oncogene. 2002;21:3934–8.
45. Catapano C, Rahm JV, Omer M, Teodori L, Kjems J, Dietz MS, Heilemann M. Biased activation of the receptor tyrosine kinase HER2. Cell Mol Life Sci. 2023;80:158.
46. Gala K, Chandarlapaty S. Molecular pathways: HER3 targeted therapy. Clin Cancer Res. 2014;20:1410–6.
47. Ruiz-Saenz A, Dreyer C, Campbell MR, Steri V, Gulizia N, Moasser MM. HER2 Amplification in Tumors Activates PI3K/Akt Signaling Independent of HER3. Cancer Res. 2018;78:3645–58.
48. Gao L, Zhang Y, Feng M, Shen M, Yang L, Wei B, Zhou Y, Zhang Z. HER3: Updates and current biology function, targeted therapy and pathologic detecting methods. Life Sci. 2024;357: 123087.
49. Jeong H, Kim J, Lee Y, Seo JH, Hong SR, Kim A. Neuregulin-1 induces cancer stem cell characteristics in breast cancer cell lines. Oncol Rep. 2014;32:1218–24.
50. Asada S, Choi Y, Yamada M, Wang SC, Hung MC, Qin J, Uesugi M. External control of Her2 expression and cancer cell growth by targeting a Ras-linked coactivator. Proc Natl Acad Sci U S A. 2002;99:12747–52.
51. Therkildsen C, Bergmann TK, Henrichsen-Schnack T, Ladelund S, Nilbert M. The predictive value of KRAS, NRAS, BRAF, PIK3CA and PTEN for anti-EGFR treatment in metastatic colorectal cancer: A systematic review and meta-analysis. Acta Oncol. 2014;53:852–64.
52. Huang L, Guo Z, Wang F, Fu L. KRAS mutation: from undruggable to druggable in cancer. Signal Transduct Target Ther. 2021;6:386.
53. Dang CV, Reddy EP, Shokat KM, Soucek L. Drugging the "undruggable" cancer targets. Nat Rev Cancer. 2017;17:502–8.
54. Zhu C, Guan X, Zhang X, Luan X, Song Z, Cheng X, Zhang W, Qin J-J. Targeting KRAS mutant cancers: from druggable therapy to drug resistance. Mol Cancer. 2022;21:159.
55. Wu X, Song W, Cheng C, Liu Z, Li X, Cui Y, Gao Y, Li D. Small molecular inhibitors for KRAS-mutant cancers. Front Immunol. 2023;14:1223433. https://doi.org/10.3389/fimmu.2023.1223433. PMID: 37662925; PMCID: PMC10470052.
56. Cefalì M, Epistolio S, Palmarocchi MC, Frattini M, De Dosso S. Research progress on KRAS mutations in colorectal cancer. Journal of Cancer Metastasis and Treatment. 2021;7:26.
57. Wang H, Chi L, Yu F, Dai H, Gao C, Si X, Wang Z, Liu L, Zheng J, Shan L, et al. Annual review of KRAS inhibitors in 2022. Eur J Med Chem. 2023;249:115124.
58. Inoue Y, Saigusa S, Iwata T, Okugawa Y, Toiyama Y, Tanaka K, Uchida K, Mohri Y, Kusunoki M. The prognostic value of KRAS mutations in patients with colorectal cancer. Oncol Rep. 2012;28:1579–84.
59. Arrington AK, Heinrich EL, Lee W, Duldulao M, Patel S, Sanchez J, Garcia-Aguilar J, Kim J. Prognostic and predictive roles of KRAS mutation in colorectal cancer. Int J Mol Sci. 2012;13(10):12153–68. https://doi.org/10.3390/ijms131012153. PMID: 23202889; PMCID: PMC3497263.
60. De Roock W, Jonker DJ, Di Nicolantonio F, Sartore-Bianchi A, Tu D, Siena S, Lamba S, Arena S, Frattini M, Piessevaux H, Van Cutsem E, O'Callaghan CJ, Khambata-Ford S, Zalcberg JR, Simes J, Karapetis CS, Bardelli A, Tejpar S. Association of KRAS p.G13D mutation with outcome in patients with chemotherapy-refractory metastatic colorectal cancer treated with cetuximab. JAMA. 2010;304(16):1812–20. https://doi.org/10.1001/jama.2010.1535. PMID: 20978259.
61. Ihle NT, Byers LA, Kim ES, Saintigny P, Lee JJ, Blumenschein GR, Tsao A, Liu S, Larsen JE, Wang J, et al. Effect of KRAS oncogene substitutions on protein behavior: implications for signaling and clinical outcome. J Natl Cancer Inst. 2012;104:228–39.
62. Cox AD, Fesik SW, Kimmelman AC, Luo J, Der CJ. Drugging the undruggable RAS: Mission possible? Nat Rev Drug Discov. 2014;13:828–51.
63. Prior IA, Lewis PD, Mattos C. A comprehensive survey of Ras mutations in cancer. Cancer Res. 2012;72:2457–67.
64. Hammond DE, Mageean CJ, Rusilowicz EV, Wickenden JA, Clague MJ, Prior IA. Differential reprogramming of isogenic colorectal cancer cells by distinct activating KRAS mutations. J Proteome Res. 2015;14:1535–46.
65. Hobbs GA, Der CJ, Rossman KL. RAS isoforms and mutations in cancer at a glance. J Cell Sci. 2016;129:1287–92.
66. Oliver JR, Kushwah R, Hu J. Multiple roles of the epithelium-specific ETS transcription factor, ESE-1, in development and disease. Lab Invest. 2012;92:320–30. https://doi.org/10.1038/labinvest.2011.186.

Publisher's Note